FISEVIER

Contents lists available at ScienceDirect

Palaeogeography, Palaeoclimatology, Palaeoecology

journal homepage: www.elsevier.com/locate/palaeo



Facies, phosphate, and fossil preservation potential across a Lower Cambrian carbonate shelf, Arrowie Basin, South Australia



Sarah M. Jacquet^{a,b,*}, Marissa J. Betts^{c,d}, John Warren Huntley^a, Glenn A. Brock^{b,d}

- ^a Department of Geological Sciences, University of Missouri, Columbia, MO 65211, USA
- b Department of Biological Sciences, Macquarie University, Sydney, New South Wales 2109, Australia
- ^c Palaeoscience Research Centre, School of Environmental and Rural Science, University of New England, Armidale, New South Wales 2351, Australia
- d Early Life Institute and Department of Geology, State Key Laboratory for Continental Dynamics, Northwest University, Xi'an 710069, China

ARTICLE INFO

Keywords: Microfacies Calcareous Organophosphatic Taphonomy Biominerals Hardgrounds

ABSTRACT

The effects of sedimentological, depositional and taphonomic processes on preservation potential of Cambrian small shelly fossils (SSF) have important implications for their utility in biostratigraphy and high-resolution correlation. To investigate the effects of these processes on fossil occurrence, detailed microfacies analysis, biostratigraphic data, and multivariate analyses are integrated from an exemplar stratigraphic section intersecting a suite of lower Cambrian carbonate palaeoenvironments in the northern Flinders Ranges, South Australia. The succession deepens upsection, across a low-gradient shallow-marine shelf. Six depositional Facies Sequences are identified ranging from protected (FS1) and open (FS2) shelf/lagoonal systems, high-energy inner ramp shoal complex (FS3), mid-shelf (FS4), mid- to outer-shelf (FS5) and outer-shelf (FS6) environments. Non-metric multi-dimensional scaling ordination and two-way cluster analysis reveal an underlying bathymetric gradient as the main control on the distribution of SSFs. Unlike groups that produced primary organophosphatic biominerals, taxa that built calcareous skeletons are more taphonomically-controlled, which is further exacerbated by sampling and processing biases. A strong facies association with condensed and reworked horizons suggests the stratigraphic occurrence of calcareous groups reflects conditions conducive to preservation (phosphogenesis and phosphatization) rather than true stratigraphic ranges. Consequently, organophosphatic taxa should take precedence in the erection of biostratigraphic zones for subdivision of lower Cambrian successions.

1. Introduction

Early Cambrian shelly faunas ("small shelly fossils" or SSF) represent a major component of Cambrian skeletospace (Thomas et al., 2000; Thomas, 2005), including both originally organophosphatic and calcareous shells. However, since acid digestion of surrounding limestone is the main extraction method for SSFs, primary calcitic and aragonitic shells (including chancelloriids, archaeocyaths, helcionelloids, bivalves, halkieriids and hyoliths) are normally destroyed, unless they have been replaced, coated or infilled with phosphate or other acid-resistant minerals.

Silicification and other post-depositional replacement via iron oxides or glauconite is relatively common in the fossil record, but the fidelity of shell replacement by these pathways, whilst variable is often coarse, and does not normally reproduce fine ultrastructural details of the original shell (Porter, 2004, though see Martí Mus et al., 2008; Jacquet and Brock, 2016). However, both phosphatization (i.e.

replacement) and localised phosphogenesis/phosphate mineralization (i.e. coating and steinkern formation) can preserve or replicate shell ultrastructures in exceptional detail, particularly in diminutive calcareous faunas (Brasier, 1990; Dzik, 1994; Porter, 2004). In the case of phosphogenesis, elevated production of phosphate tends to be associated with smaller particles—within a range of $\sim 80-\sim 350\,\mu m$ —that have low ambient pore-water oxygen causing oscillating redox conditions conducive to precipitation (Pruss et al., 2018). This "SSF-style preservation" biases preservation of fossils with small internal pore or void spaces and is responsible for steinkern formation.

Phosphatic replacements, coatings, and steinkerns of shelly faunas are commonly associated with Cambrian deposits. Geochemical studies of Cambrian Series 2–3 Thorntonia Limestone in western Queensland, Australia suggest the source of sedimentary phosphorus is linked to organic matter and iron oxide remobilization in an anoxic, reducing environment (Creveling et al., 2014a, 2014b). However, SSF-style preservation occurs throughout the Phanerozoic (Creveling et al.,

^{*} Corresponding author at: Department of Geological Sciences, University of Missouri, Columbia, MO 65211, USA. *E-mail address:* jacquets@missouri.edu (S.M. Jacquet).

2014a, 2014b; Dattilo et al., 2016; Frauhiger et al., 2018; Pruss et al., 2018). Lower Triassic successions from Nevada, USA reveal that oscillating pore-water redox during periods of prolonged oxygen depletion is instrumental in phosphate nucleation during early diagenesis (Pruss et al., 2018). Whilst this research provides crucial insight into microenvironmental conditions associated with phosphogenesis and the preservation of calcareous SSF, studies into broader sedimentological, depositional and taphonomic processes controlling the stratigraphic and spatial variation of calcareous and organophosphatic SSF are lacking.

For most SSF biostratigraphic studies—particularly in the Cambrian—fossil material is primarily recovered using acid maceration techniques. For calcareous taxa, largely destroyed using such techniques, stratigraphic reports become sporadic, and depending on preservational conditions, phosphatic steinkerns of dissolved calcareous shells can dominate taxonomic relative abundance in individual horizons (Landing, 1988; Landing et al., 1989; Landing and Bartowski, 1996; Gravestock et al., 2001; Steiner et al., 2004; Skovsted, 2006; Parkhaev and Demidenko, 2010; Devaere et al., 2013; Yang et al., 2014; Kouchinsky et al., 2015; Betts et al., 2016; Betts et al., 2017). These intervals may yield hundreds of individual fossils, whilst abundance in adjacent horizons can be very low. For taxa that accrete an organophosphatic shell, there is an inherent observational bias since these biominerals remain unaffected by acid maceration processes. The stratigraphic distribution of calcareous and organophosphatic SSF relative to that of elevated phosphate deposition and other lithological characteristics is rarely quantified.

Here we provide a case study from the lower Cambrian (late Terreneuvian Stage 2, and Series 2, Stage 3) Hawker Group in the northern Flinders Ranges of South Australia. Detailed microfacies analyses were conducted on carbonates in the Moro Gorge (MOG) section (base of section: 30°43.313'S; 139°11.991'E) in order to interpret depositional facies sequences in a typical low latitude epeiric carbonate succession developed in early Cambrian East Gondwana. This sedimentological framework provided context for subsequent multivariate analyses of the palaeontological data, principally fossils recovered in acid residues, though thin sections also demonstrate the occurrence of calcareous forms along the section. Herein, we test the hypothesis that the stratigraphic distribution of both organophosphatic and calcareous skeletal fossils is predictably associated with specific lithofacies and/or depositional environments. The implications of potential facies dependence coincident with broader taphonomic constrains on shelly fossil preservation is discussed in terms of the impact on regional biostratigraphy and global correlation.

2. Materials and methods

Palaeontological and lithological samples were collected along a 589.7 m (true thickness) measured stratigraphic section (MOG, Figs. 1–3, see also Betts et al., 2016, fig. 5, appendix 4). A total of 57 oriented rock samples were collected along the MOG section for petrological thin section. Thin sections were imaged in plane polarised and crossed polarised light using a Nikon Eclipse 50ipol microscope with associated NIS Elements Documentation software in the Department of Earth and Planetary Sciences, Macquarie University. Both thin sections and rock slabs from each horizon were polished for geochemical analyses. Select samples were examined under back-scattered scanning electron microscopy and energy dispersive spectroscopy using a Zeiss EVO MA15 scanning electron microscope (with Oxford Instruments Aztec Synergy EDS/EBSD), whist additional polished hand samples were examined using a Bruker M4 Tornado micro-XRF with a Rh anode tube and dual Bruker silicon drift detector energy dispersive spectrometers.

Shelly fauna were extracted using standard acid leaching protocols (Jeppsson et al., 1999) where limestones are dissolved in 10% acetic acid, extracting acid-insoluble microfossils, including primary

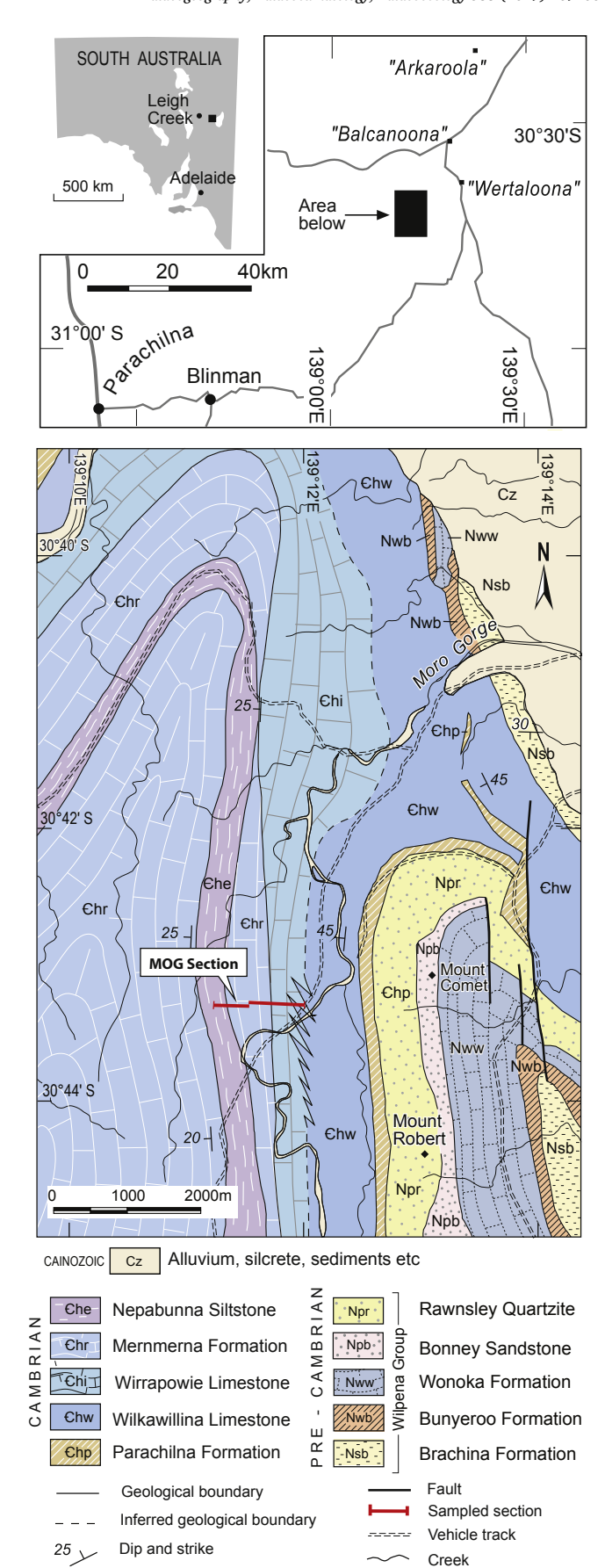


Fig. 1. Regional locality and detailed geology of the eastern limb of the Arrowie Syncline, Flinders Ranges, South Australia.

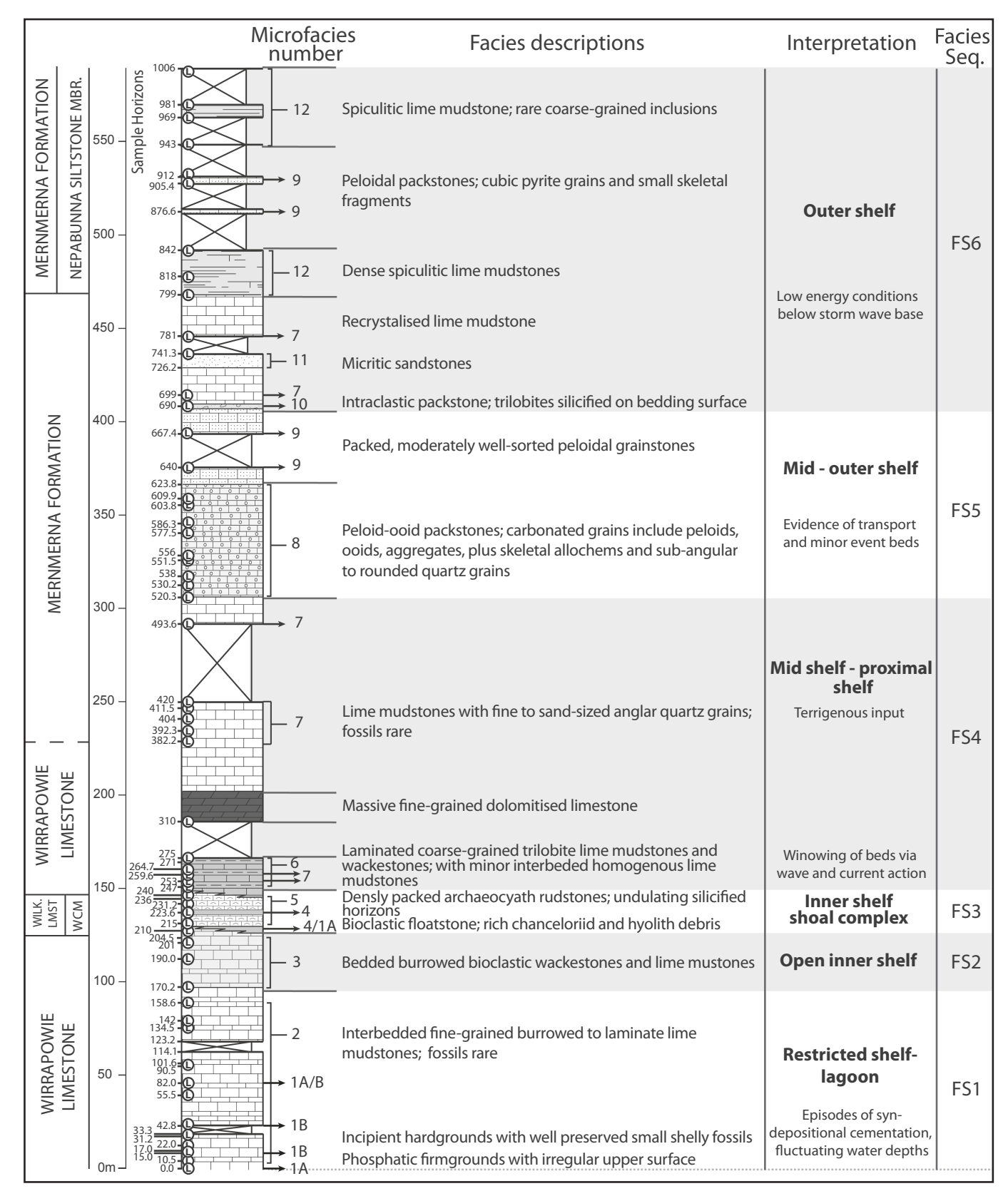


Fig. 2. Lithostratigraphic section with description of main facies types in MOG section (base of section: 30°43.313′S; 139°11.991′E; top of section: 30°43.333′S; 139°43.333′E) and interpretation of depositional environments. Microfacies numbers correspond to: 1A = phosphatic firmground; 1B = incipient hardground; 2 = burrowed-laminate lime mudstones; 3 = burrowed bioclastic wackestones; 4 = bioclastic floatstones; 5 = archaeocyath rudstones; 6 = trilobitic wackestones; 7 = lime mudstones; 8 = peloid-oolitic packstone; 9 = peloidal packstone; 10 = intraclastic packstone; 11 = micritic sandstone; 12 = spiculitic lime mudstone. Facies seq = facies sequence.

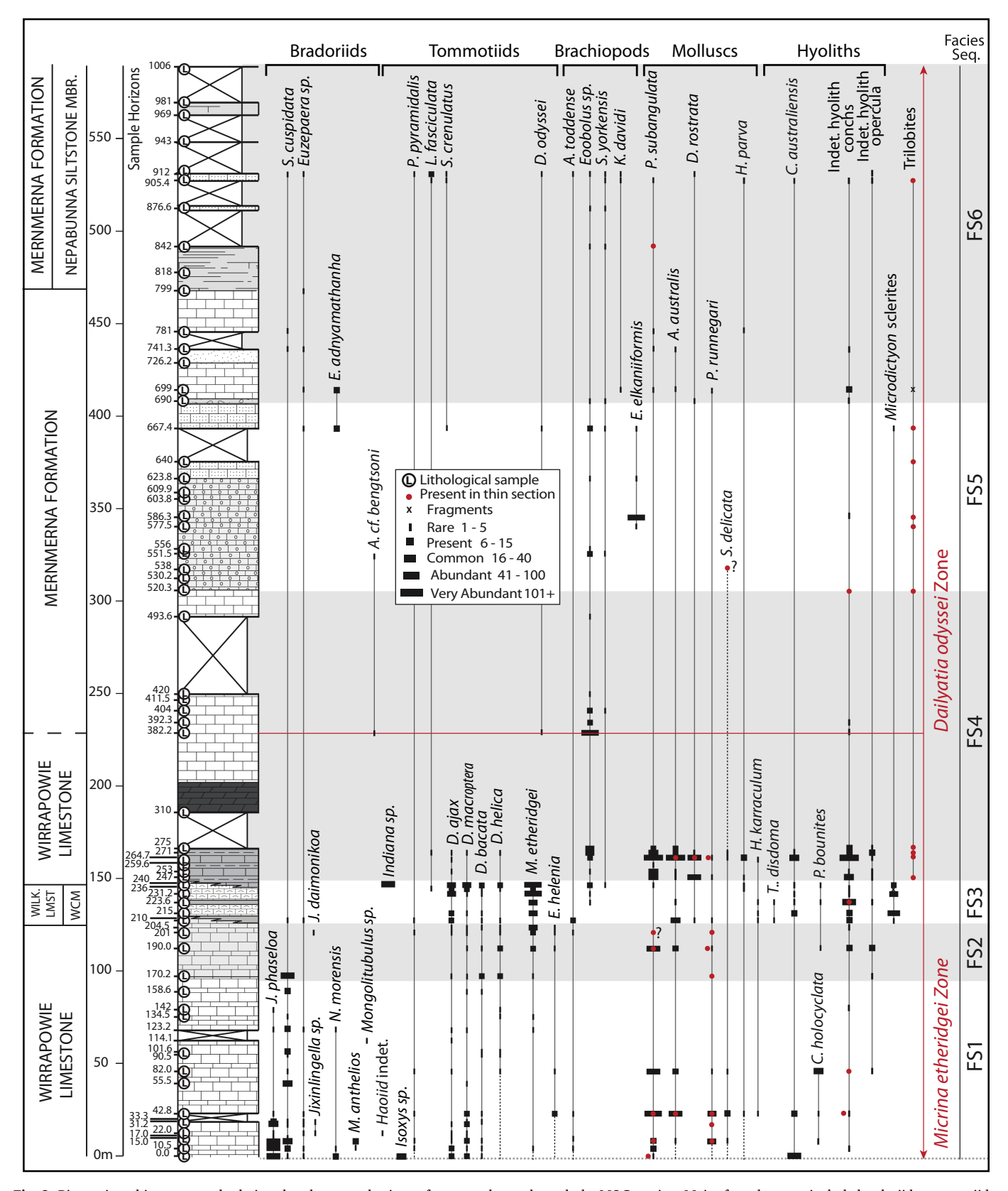


Fig. 3. Biostratigraphic ranges and relative abundance per horizon of recovered taxa through the MOG section. Major faunal groups include bradoriids, tommotiids, brachiopods, molluscs, hyoliths, *Microdictyon* sclerites, and trilobites. Facies sequences indicated on right-hand side.

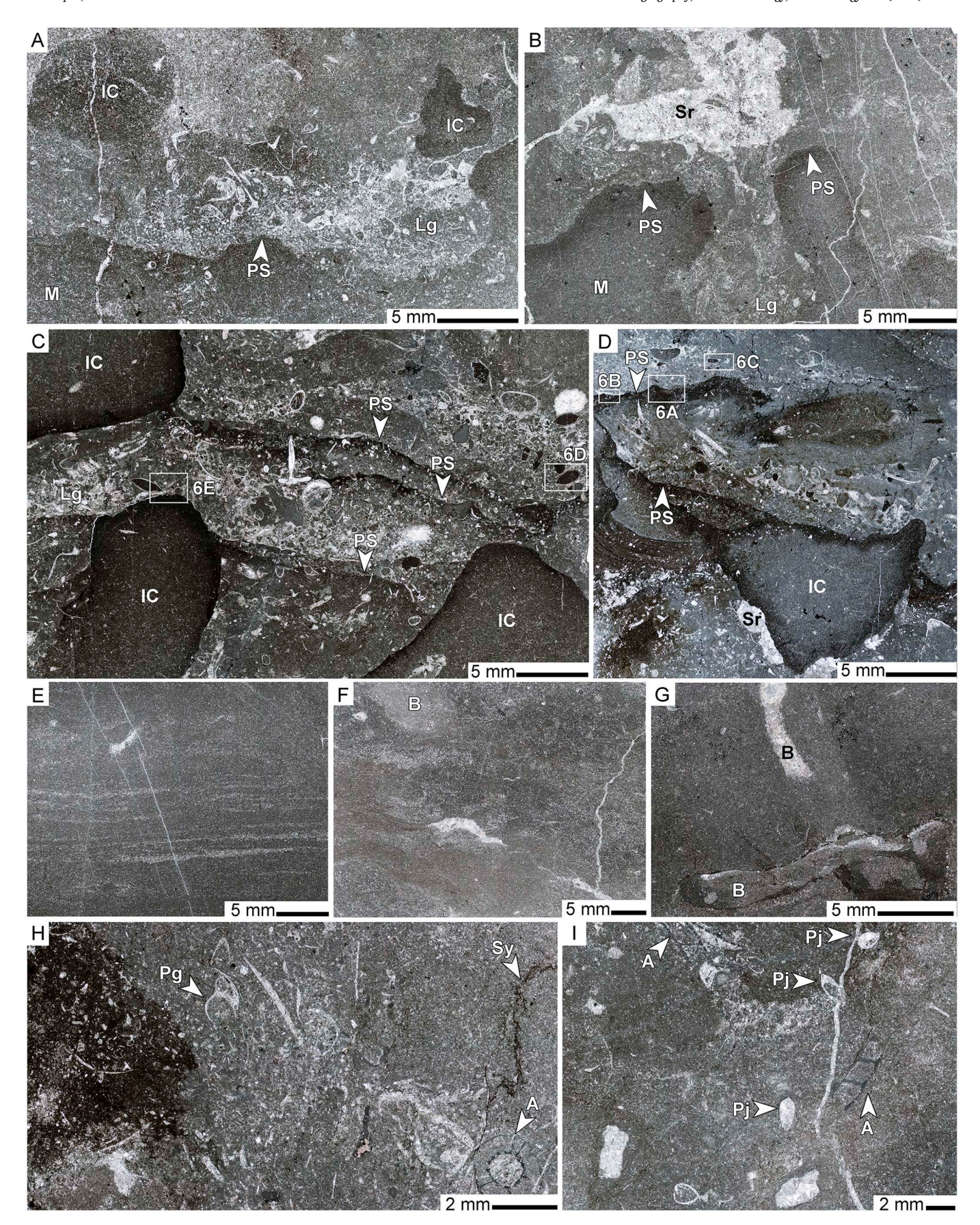


Fig. 4. Lithofacies types from FS1 and FS2 (Wirrapowie Limestone). A–B. Phosphatic firmgrounds (Microfacies 1A). A. MOG/0.0. B. MOG/82.0. C–D. Incipient hardgrounds (Microfacies 1B). C. MOG/15.0. D. MOG/42.8. E–F Laminated-burrowed mudstone (Microfacies 2). E. MOG/22.0. F. MOG/31.2. G. MOG/10.5. H–I. Burrowed bioclastic wackestone (Microfacies 3). H. MOG/190.0. I. MOG/201.0. Abbreviations: PS = phosphatic surface, IC = intraclast, M = micrite, LG = lag deposit, Sr = spar, B = burrow, Pg = Pelagiella, Sy = stylolite, Sy = s

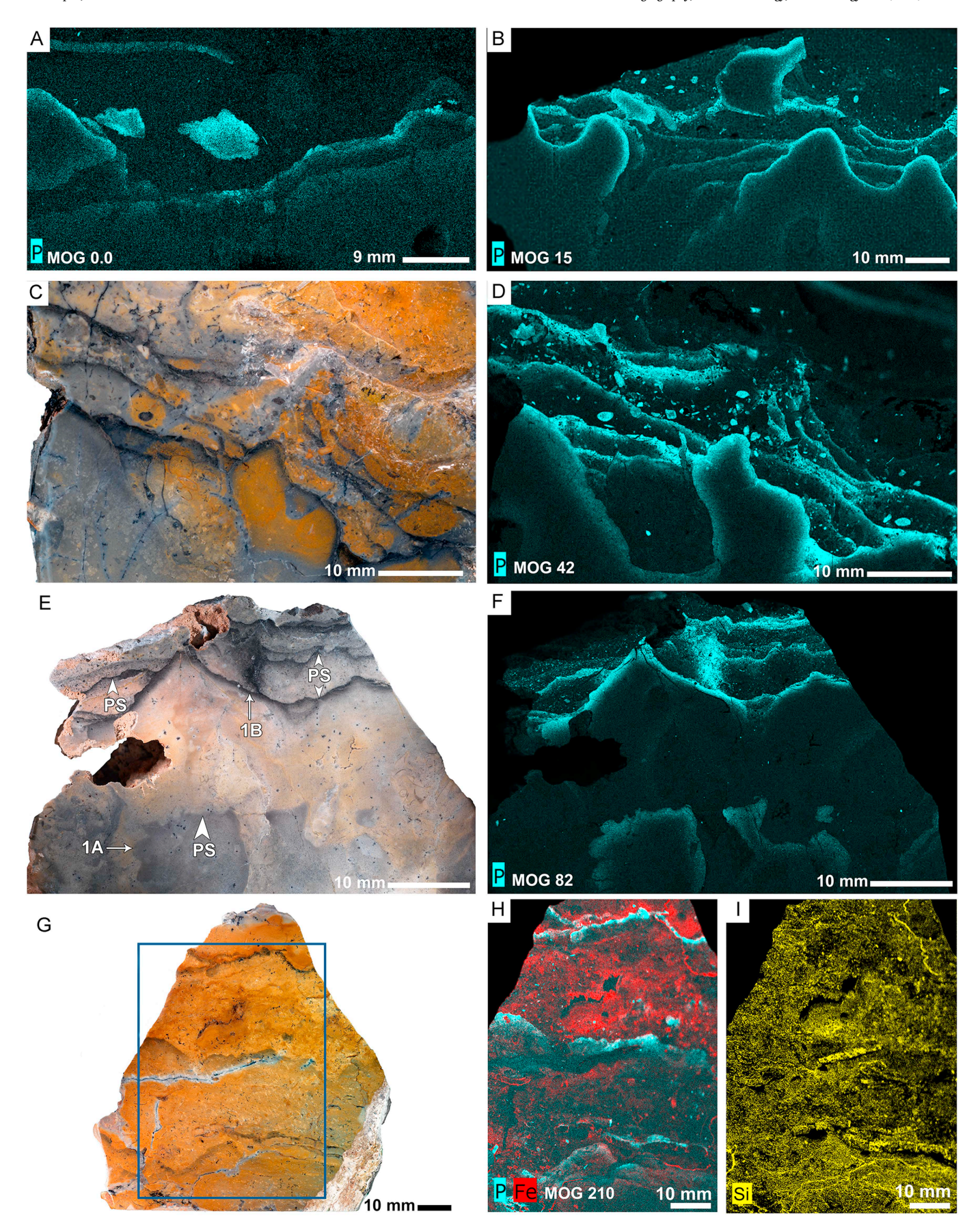


Fig. 5. Polished blocks and elemental maps from EDS analysis showing areas of phosphate enrichment and penetration in firmground and hardground samples. A. Phosphate map of MOG/0.0, Microfacies 1A. B. Phosphate map of MOG/15, Microfacies 1B. C–D. Polished section of sample MOG/42 (C), Microfacies 1B and corresponding EDS map (D). E–F. Polished section of sample MOG/82 (E), Microfacies 1A and 1B and corresponding EDS map (F). G–I. Polished section of sample MOG/210 (G), Microfacies 4/1A and corresponding EDS maps (H, I).

organophosphatic and siliceous biominerals, secondarily replaced phosphatized or silicified skeletal elements, and phosphatic steinkerns or coatings. Residues were sieved (63 μm and 250 μm fractions retained), washed using de-ionised water and oven dried ($\sim\!50\,^{\circ}\text{C}$) before examination and picking under a stereo binocular microscope. Selected specimens were placed on pin stubs and gold sputter coated prior to imaging using a JEOL JSM-6480LA Analytical Scanning Electron Microscope in the Microscopy Unit at Macquarie University.

Insoluble fossiliferous content from acid residues was picked and counted to determine relative abundance and stratigraphic distribution of skeletal elements throughout the MOG section. For the calcareous biota, only molluscs (including helcionelloids, halkieriids and bivalves) and hyoliths were used for the following analyses. Due to the often disarticulated and fragmentary nature of both chancelloriids and archaeocyathids, these sessile taxa where excluded from statistical analyses. Three main groups of organophosphatic fauna were quantified; tommotiids, phosphatic brachiopods and bradoriids. Calcareous skeletal taxa are composed of either one or two elements, whereas all organophosphatic faunas (plus the halkieriids) have two or more elements. For the multielement taxa each skeletal component was counted (valve, shield or sclerite) as separate elements (unless conjoined), and identifiable fragments were included as single individuals.

In total, 3936 individual skeletal elements from 45 taxa and 67 samples were picked from acid residues from the MOG section, with sub-equal parts calcareous (n=1973) and organophosphatic (n=1963) (Appendix A). In order to minimize the undue influence of small samples in subsequent multivariate analyses, this matrix was filtered by removing samples and taxa with fewer than five specimens, resulting in a matrix of 3893 specimens from 38 taxa and 44 samples (representing 98.9% of the total number of individuals; calcareous n=1966, organophosphatic n=1927).

A non-metric multi-dimensional scaling ordination (nMDS) was applied to the filtered matrix of taxon abundance to determine any underlying environmental gradient controlling taxon distribution. Since the specimen counts have not been corrected to reflect the minimum number of individuals (due to the inherent uncertainty for the multi-element taxa), it is prudent to determine the sensitivity of the nMDS ordination to such counts. To this end, a second nMDS ordination was conducted on the presence/absence data derived from the filtered taxon occurrence matrix. These ordinations were conducted using the Bray-Curtis dissimilarity index and the matrix was reduced to three dimensions. The nMDS was conducted in *R* 3.4.1 "Single Candle" (*R* Core Team, 2017) using the *metaMDS* function in the *vegan* package (Oksanen et al., 2017).

A two-way cluster analysis, using the UPGMA algorithm and Bray-Curtis similarity index in PAST v. 3.22, was conducted on the filtered matrix of taxon abundance to explore the relationships between taxon abundance, preservation mode, microfacies, and depositional facies sequence. The resulting matrix plot shows the number of specimens in each sample. Taxa are displayed on the vertical axis and are colour coded by preservation. Samples are displayed on the horizontal axis and labelled by facies sequence and microfacies.

3. Locality and stratigraphy

Palaeontological and petrographic samples were systematically collected along the MOG section (Figs. 2, 3) that intersects a wide spectrum of carbonate lithologies within the *Micrina etheridgei* Zone and overlying *Dailyatia odyssei* Zone established by Betts et al. (2016, 2017, 2018). The base of the MOG section (coordinates: 30°43.313′S; 139°11.991′E) is located 5 km south of Moro Gorge on the NE limb of the Arrowie Syncline, northern Flinders Ranges (Fig. 1). The MOG section transects approximately 589.7 m (true thickness) of carbonate facies within the Wirrapowie Limestone, Wilkawillina Limestone (Winnitinny Creek Member) and Mernmerna Formation (including Nepabunna Siltstone Member) (Figs. 2, 3).

3.1. Wirrapowie Limestone

The lowest 127.4 m of the MOG section intersects fine-grained, light blue-grey, massive to bedded limestones and microbialites typical of the Wirrapowie Limestone. The majority of this interval is sparsely fossiliferous (Fig. 3), though rare incipient hardground facies (see below) preserve rich shelly fossil debris visible in hand specimen (Figs. 4, 5). These incipient hardgrounds in addition to phosphatic firmgrounds represent minor, but distinctive omission surfaces in the lower 45.9 m of the section (Fig. 2). Lithologically, this interval is very similar to the Wirrapowie Limestone type section described by Haslett (1975) which is free from desiccation cracks, cross beds and coarse detrital material (as in the MOG section). However, intermittent grainstone beds and stromatolites evident in the type section (Haslett, 1975, p. 217) are not well represented in the MOG section.

3.2. Wilkawillina Limestone (Winnitinny Creek Member)

Immediately above MOG/210 (127.4 m true thickness above the base of the section) the lithology consists of a 23.2 m-thick package of prominent, massive bioclastic packstones and rudstones with interbedded silicified muddy layers. Archaeocyath fragments and hyoliths are visible on the surface of silicified horizons. The distinctive archaeocyath rudstones are very similar to those described from the Winnitinny Creek Member in the MORO section (Betts et al., 2014, 2016) and the Winnitinny Creek Member in the type section of the Wilkawillina Limestone in Wilkawillina Gorge in the Bunkers Graben (Clarke, 1986a, 1986c, 1990a). At MOG/247.0, 150.6 m above the base of the section, archaeocyath rudstones are conformably overlain by a 78.19 m-thick package of clean, finely bedded micritic limestones interbedded with thin (millimetric) layers of fine grained angular to subrounded quartz grains, potentially representing a return to Wirrapowie Limestone facies.

3.3. Mernmerna Formation

The contact between the Wirrapowie Limestone and the conformably overlying Mernmerna Formation is obscured in the MOG section by poor outcrop and a dolomitised interval from 166.2 to 199.2 m above the base of the section. The incoming of Dailyatia odyssei at 228.8 m true thickness (MOG/382.2, Fig. 3) represents the base of the eponymous biozone (Betts et al., 2016, 2017). The lower 77.2 m of the Mernmerna Formation (where outcropping) consists of blue, micritic limestones with intermittent tempestites. These are overlain by a 60.4 m-thick package of oolitic and peloidal limestones (Fig. 2). At 366.4 m above the base of the section (MOG/623.8), the lithology returns to dark blue-grey micritic limestones, interbedded with occasional beds of intraclastic conglomerates, and sandy layers with interstitial muds (Fig. 2). In the type section in the Bunkers Range the two lower members of the Mernmerna Formation (Six Mile Bore Member and Linns Springs Member) are identified by flaggy limestones with slump folds, turbidites and intraformational truncation indicative of deposition on an unstable slope in deeper water (Clarke, 1986c, 1990b). Whilst these sedimentary features are not apparent in the MOG section, the sequence described above is indicative of a gradual deepening consistent with the transgressive deposits of sedimentary sequence ε 1.2 in the Arrowie Basin (Gravestock and Cowley, 1995; Zang et al., 2004).

3.4. Mernmerna Formation (Nepabunna Siltstone Member)

At 467.9 m true thickness above the base of the section, a 121.7 m package of calc-mudstones rich in sponge spicules and pyritic peloidal grainstones characterise the Nepabunna Siltstone Member of the Mernmerna Formation. This unit is sparsely fossiliferous with only a few compressed indeterminate hyolith conchs and large tubes

recovered (GAB pers. obsv) and only crops out as a mappable unit in the Arrowie Syncline. Most shelly fauna are associated with turbidity flows in the form of peloidal grainstones shed from the adjacent shelf.

4. Microfacies and depositional Facies Sequences (FS)

Microfacies analyses provide context for quantifying the distribution of skeletal elements throughout the section in relation to environmental and lithofacies associations. Twelve carbonate microfacies are represented in the MOG section (Fig. 2) through the Wirrapowie Formation, Wilkawillina Limestone, and Mernmerna Formation. We also interpret six depositional Facies Sequences (FS) (Fig. 2). Some microfacies occur repeatedly throughout the section and in different lithological formations (Fig. 2). Description of microfacies follows the emended Dunham classification of limestones (Wright, 1992); see also (Flügel, 2004).

4.1. Facies Sequence 1 (FS1): Wirrapowie Limestone

Facies Sequence 1 is interpreted as a shallow subtidal semi-restricted shelf or lagoonal environment on the inner-shelf, prone to periods of non-deposition and reduced sedimentary input. This sequence package is 97.3 m thick, with characteristic facies including lime mudstones, with distinctive condensed surfaces including phosphatic firmgrounds (Microfacies 1A) and incipient hardgrounds (Microfacies 1B) that together constitute 2.9% of the section. Microfacies 2 is a burrowed-laminated lime mudstone that makes up 14.3% of the section (Figs. 2, 4A–B). Repetition of interbedded bioturbated-laminated lime mudstones suggests subtidal settings with intermittent fluctuation in oxygen availability at the sediment-water interface (Flügel, 2004).

Microfacies 1A is represented by recurrent firmgrounds (MOG/0.0, MOG/82, Figs. 4A, B, 5A, E-F) characterised by sharp, but topographically complex, erosional upper surfaces penetrated by phosphate (Fig. 5A, F, H). Underlying facies typically represent sparse wackestones with skeletal allochems randomly oriented and dispersed within the matrix (Fig. 4A). The phosphatic surfaces are overlain by a mosaic of micrites and sparry calcites. Skeletal debris is abundant and concentrated above the topographic lows (i.e. pits, grooves and fissures) of the phosphatic surface (Fig. 4A). Some skeletal components preserve geopetal features and are mostly replaced or infilled by microspar. Subangular to subrounded carbonate rip-up clasts (>9 mm in diameter) from the underlying lime mudstones are often entrained within the overlying fabric. These horizons are distinct from the well-developed incipient hardgrounds (Figs. 4C-D, 5B-F) in possessing a single phosphatic surface. However, they can be found in close association with these more condensed surfaces, for instance in MOG/82 (Fig. 5E-F).

Incipient hardgrounds (Microfacies 1B, MOG/15 and MOG/42.8, Figs. 2, 4C-D, 5B-F, 6A-E) display complex fabrics with repeated, and often laterally discontinuous phosphatic omission surfaces. The incipient hardgrounds display fabrics of irregular thickness (ranging between 1 and 7 mm), composed of fining-upwards, packed skeletal-intraclastic wackestones. Energy dispersive X-ray spectroscopy analysis reveals the phosphatic upper surfaces are undulose, with greater phosphate concentrations penetrating deeper into the underlying skeletal micrite (Figs. 5B, D, F, 6A-B [P = phosphorus]). Skeletal allochems are abundant within the hardground and overlying lag deposits, typically infilled with micrite or drusy-blocky spar. Shells are also clearly infilled by phosphate (fluorapatite) forming steinkerns (Figs. 4C-D, 5B-D, 6B-D). Identifiable shells consist of molluscan taxa including the bivalve Pojetaia runnegari Jell, 1980 and coiled helcionelloid, Pelagiella subangulata Tate, 1892 (identified principally on the basis of its abundance in acid residues), in addition to a number of indeterminate hyolith conchs. Other fauna include abundant chancelloriid sclerites, hexactinellid spicules, archaeocyath fragments, and rare organophosphatic brachiopods. Shelly debris is commonly concentrated in the overlying phosphatic surfaces as lag deposits (Figs. 4C, 5B–D), sometimes entrained within sparry cement in conjunction with well-rounded sand-sized quartz grains (Fig. 6A–B [Si]) and intraclasts (0.3–1 mm in diameter). Skeletal allochems are poorly sorted with random orientation, and only rarely project across phosphatic surfaces. Counts of the skeletal elements with conical, pennate and cap-shaped morphologies in Microfacies 1B (MOG/42.8, Fig. 4D) reveals that 28% were infilled by phosphate forming steinkerns, and the remaining 72% were either infilled with micrite (61%) or occluded by blocky calcite (11%).

In MOG/15, reworked, marginally phosphatized intraclasts (Fig. 6E [P]) are randomly oriented and entrained into the laminate microfacies, and represent up to 30% of the fabric (Fig. 4C). Intraclasts consist of consolidated micritic matrix with rare skeletal inclusions. Cavities immediately adjacent to, or underneath the intraclasts, are infilled with blocky and fibrous calcite cements (Fig. 4D).

The fine-scale vertical stacking of phosphatic surfaces in incipient hardground facies (Fig. 4C-D) may have formed in environments influenced by repeated minor fluctuations in depth, (similar to surfaces described from the Ordovician of Öland (Nordlund, 1989)). The incipient hardground surfaces from the MOG section display little to no evidence of subaerial exposure, such as microkarst, enriched ironoxides on the omission surface, dolomitisation or meteoric (vadose) cementation (Hillgaertner, 1998; Palmer et al., 1988), suggesting the hardgrounds were most likely consistently submerged. The firmground and incipient hardground surfaces with increased phosphatic penetration (e.g. MOG/42.8, Figs. 4D, 5A-B, D, F, 6A-B [P]) indicate prolonged exposure at the sediment-water interface with little or no sediment input and accumulation. Microfacies indicate a low energy semi-restricted to protected environment, with recurrent episodes of reduced oxygen and sediment input. Firmground and hardground facies have been reported in lagoonal settings but can be associated with shallow shoals and carbonate shelf or mid-shelf settings (Christ et al., 2015, references therein).

Microfacies 2 (burrowed-laminated lime mudstone, Fig. 4E–G) constitutes the dominant lithology in FS1 and is interbedded between the phosphatic firmgrounds and incipient hardgrounds from 0 to 97.4 m above the base of the MOG section (Fig. 2). The fabric consists of laminated (Fig. 4E), mottled, to nodular micrites (Fig. 4F). Skeletal elements are rare (mostly siliceous sponge spicules) orientated parallel to bedding. Bioturbation is indicated by narrow elongate haloes of compressed burrows and occasional void spaces left by burrows subsequently infilled by drusy spar (Fig. 4F, G). Solution seams, stylolaminated fabrics, and calcite veining are common.

4.2. Facies Sequence 2 (FS2): Wirrapowie Limestone

Facies Sequence 2 is characterised by a distinctive, burrowed and fossiliferous 30 m-thick interval suggestive of a well-oxygenated open shelf environment. Facies include burrowed bioclastic wackestone (Microfacies 3, Figs. 2, 4H–I) comprising 4.4% of the lithofacies in the section. A high, localised abundance of *Micrina etheridgei* has generally been associated with shallow-water, moderate to high-energy environments proximal to biohermal facies (James and Gravestock, 1990; Gravestock and Cowley, 1995; Holmer et al., 2008). This is further supported by the occurrence of large archaeocyath fragments entrained in the wackestones as a result of transportation within a moderate to high-energy subtidal shelf environment on the inner platform (Fig. 4I).

This interval from 97.3 to 127.4 m above the base of the section features mottled to nodular fabrics with micritic and minor spar matrices. Calcareous skeletal allochems (bivalves, hyoliths, chancelloriids and archaeocyath fragments) are randomly oriented, dispersed and reworked throughout due to bioturbation. Skeletal allochems are secondarily replaced or infilled by calcite (Fig. 4I), and phosphatic steinkerns are rare. Small intraclasts within micrite are often recrystallized,

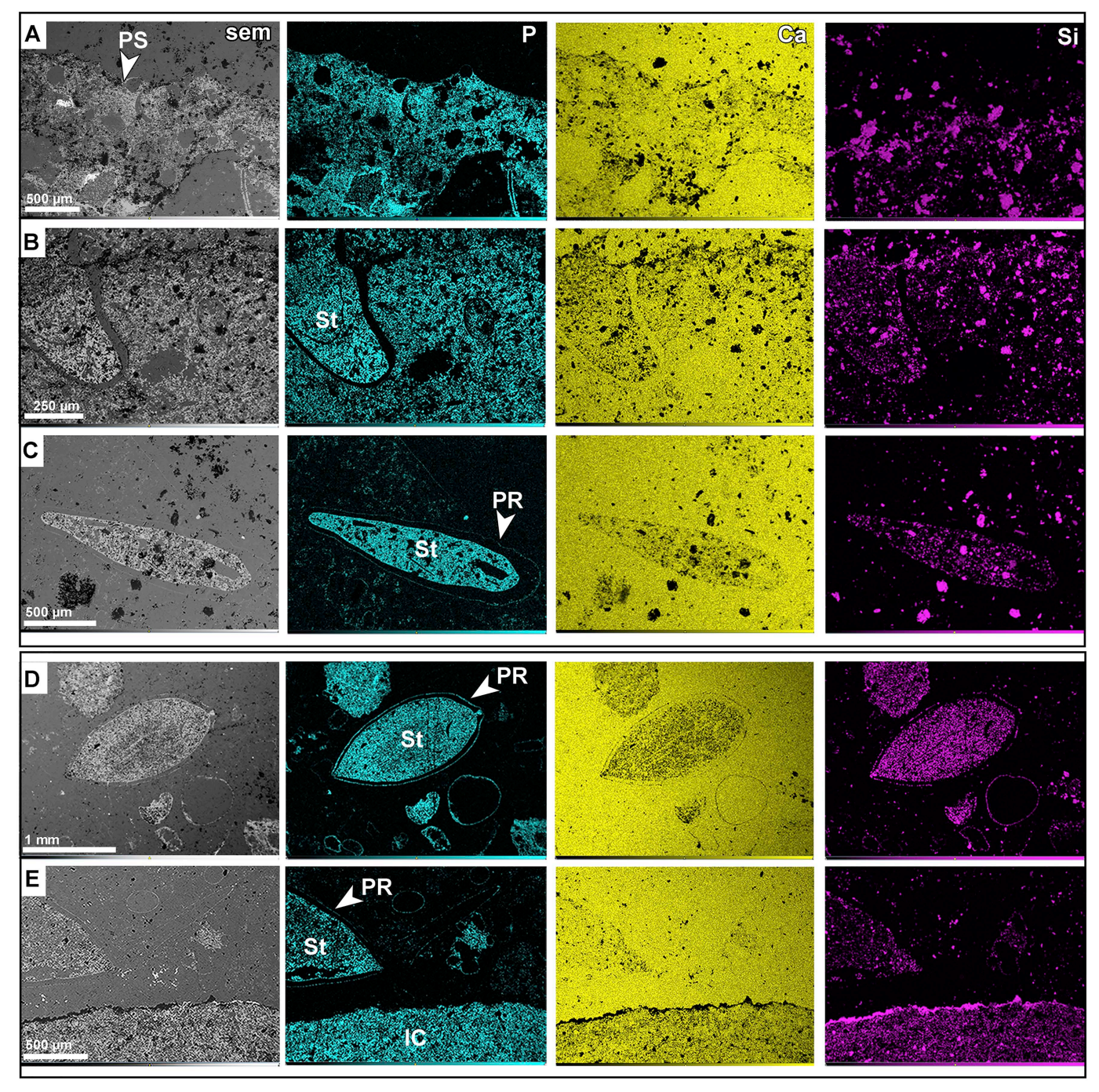


Fig. 6. Elemental maps from EDS analysis of incipient hardground facies in FS1. A–C. MOG/42.8. A. Phosphatized omission surface. B. Phosphatized omission surface with entrained helcionelloid shell. C. Cross-section of an indeterminate helcionelloid. D–E. MOG/15.0. D. Cross-section of *P. runnegari*. E. Marginally phosphatized intraclast (IC, arrow) and partial cross-section of *P. runnegari* on left-hand side. Abbreviations: St = steinkern (phosphatic), PR = phosphatic rim, PS = phosphatic surface, IC = intraclast.

and stylolites, calcite veining and interparticle precipitation of ferruginous minerals is common.

4.3. Facies Sequence 3 (FS3): Wilkawillina Limestone

Facies Sequence 3 is interpreted as being deposited within fair-weather wave base, in a moderate to high-energy subtidal environment on the inner-shelf. This is a relatively narrow stratigraphic interval (23.2 m thick) that most likely corresponds to shoaling of archaeocyath-calcimicrobial bioconstructors eroded as talus from nearby bioherms or mounds. Facies Sequence 3 includes bioclastic floatstone (Microfacies

4, 1.4% of the section, Figs. 2, 7A-C), and archaeocyath rudstone (Microfacies 5, 2.5% of the section. Figs. 2, 7D).

Microfacies 4 is characterised by a packed, poorly-sorted mosaic of chancelloriid sclerites, hexactinellid spicules and archaeocyath fragments entrained in a micritic matrix. Occasional large archaeocyath fragments (>24 mm) with septal chambers in addition to worn, submillimetric archaeocyath debris are common (Fig. 7B), whilst hyoliths (mostly conchs) constitute other minor components. Geopetal structures have formed in archaeocyath septal chambers and also occur as umbrella voids (Fig. 7B). Elongate archaeocyath fragments generally orient sub-parallel to probable bedding. Though bedding is not

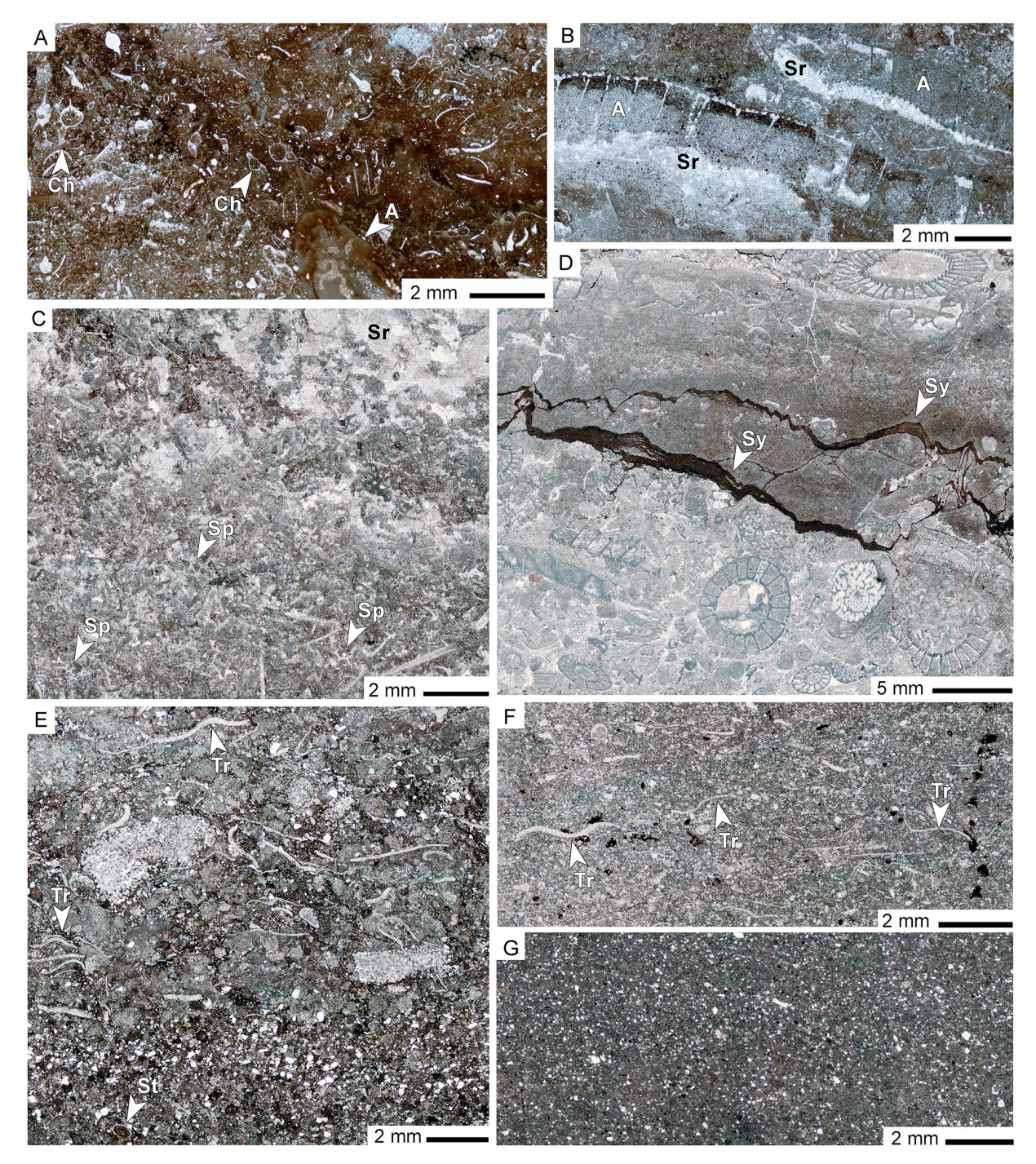


Fig. 7. Lithofacies types from FS3 (Wilkawillina Limestone, Winnitinny Creek Member) and FS4 (Wirrapowie Limestone and Mernmerna Formation). A–C. Bioclastic floatstone (Microfacies 4). A. Chancelloriid spicules entrained within iron-stained matrix, B. Large archaeocyath fragment with spar-infilled umbrella voids; MOG/210.0. C. MOG/223.6. D. Archaeocyath rudstone (Microfacies 5), MOG/236. E–F. Trilobitic wackestone (Microfacies 6). E. MOG/247.5. F. MOG/275.0. G. Lime mudstone (Microfacies 7). MOG/382.2. Abbreviations: Ch = chancelloriid, A = archaeocyath, Sr = spar, Sp = siliceous spicule, Sy = stylolite, Tr = trilobite, St = steinkern (phosphatic).

apparent in thin section, horizon MOG/210 exhibits undulating darkened surfaces that are enriched in phosphate akin to Microfacies 1A, and are most conspicuous in polished hand samples (Fig. 5G–H). These beds have also been partially to heavily silicified (Fig. 5I).

Microfacies 5 (archaeocyath rudstone, Fig. 7D) features densely-packed, poorly-sorted fragmentary and complete skeletal allochems composed predominantly of irregular and regular archaeocyaths. Sponge spicules and hyoliths are also present, but feature as a minor component. Skeletal allochems are entrained within mottled micrites and drusy-blocky sparites, often showing geopetal and umbrella voids

infilled by equant, drusy and blocky spar. High amplitude microcolumnar stylolites and anastomosing microstylolite sets occur subparallel to bedding and cross-cut archaeocyath allochems.

Heterogenous fabrics include geopetal signatures in both complete and fragmented randomly orientated archaeocyath skeletons, which suggest some transport prior to deposition. There is no evidence of in situ calcimicrobial cementation, primarily in the form of *Renalcis* and *Epiphyton*, which are usually more prevalent in the core of archaeocyath build-ups and rare in reworked deposits (James and Gravestock, 1990; Betts et al., 2014).

This depositional facies sequence bears close similarities to the skeletal grainstones, packstones and wackestones characteristic of interbiohermal facies in the Winnitinny Creek Member of the Wilkawillina Limestone in the Bunkers Graben and Range (Clarke, 1986a, 1986b, 1990a). Onlap of bioclastic floatstones and archaeocyath rudstones at level MOG/210.0 (127.4 m true thickness) marks the transition to a higher-energy environment prone to re-suspension, transport and shoaling.

4.4. Facies Sequence 4 (FS4): Wirrapowie Limestone to Mernmerna Formation transition

Facies Sequence 4 is relatively thick (155.4 m true thickness) and is interpreted as a transition from a mid-shelf to proximal shelf environment influenced by wave and current action resulting in winnowing, sorting and reworking. At the base (MOG/247), this facies sequence transitions from the inner-shelf skeletal shoal complex of FS3, into laminated, coarse-grained trilobite lime-mudstones and wackestones that define FS4. Facies Sequence 4 includes Microfacies 6 (trilobitic wackestone, 4.9% of the section, Figs. 2, 7E–F) and Microfacies 7 (lime mudstone, 13.2% of the section, Figs. 2, 7G).

Microfacies 6 is characterised by interbedded, loosely packed wackestones with sutured to stylobrecciated intraclastic fabrics (Fig. 7E) and lime mudstones with a micritic matrix (Fig. 7F). Allochems consist mostly of trilobites and brachiopod shells oriented parallel to bedding in loosely-packed layers a few millimetres thick. Rare phosphatic steinkerns are present as transported bioclasts in coarsergrained layers (Fig. 7E). Abundant sand-sized angular quartz grains are dispersed throughout the fabric.

Microfacies 7 (Fig. 7G) occurs in both FS4 and FS6. This microfacies consists of dark micrites with fine to sand-sized angular to sub-rounded quartz grains dispersed throughout the matrix. Skeletal allochems (mostly trilobites) are rare. A small package (36.7 m thick, 6.2% of the section) of massive, fine-grained dolomitised limestone occurs below the more common lime mudstones associated with FS4.

The presence of poorly-sorted sand-sized, angular to sub-angular quartz grains indicates episodic input from a proximal terrigenous source. Parallel orientation of well-preserved trilobite allochems (Fig. 7F) suggests proximal current or wave-induced winnowing of deposits below fair-weather wave base (Westrop, 1986; Fürsich and Oschmann, 1993). Upper parts of FS4 transition into finer-grained quartz-rich lime mudstones with a paucity of fossil material.

4.5. Facies Sequence 5 (FS5): Mernmerna Formation

Facies Sequence 5 is interpreted as being deposited on a mid-to outer-carbonate shelf setting below storm wave base. This 102.2 m-thick succession of peloid-ooid packstones (Microfacies 8, 11.8% of the section, Figs. 2, 8A–C) and peloidal packstones (Microfacies 9, 11% of the section, Figs. 2, 8D–F) contains moderately to well-sorted nongraded fabrics (Fig. 8B), occasionally with sharp erosional bases or internal laminae (Fig. 8A, C).

Microfacies 8 is characterised by carbonate peloids, ooids, aggregates and skeletal components as well as sub-angular to rounded fine quartz grains entrained in a micritic matrix. Fabrics are poorly to moderately well-sorted, and weakly- to moderately-compacted. Carbonate intraclasts are small (0.17–0.79 mm), sub-rounded, occurring within a micritic matrix (Fig. 8A, B). Aggregate grains (<2.5 mm across) contain a mixture of ooids, peloids, and angular quartz grains (Fig. 8C). Ooids have radial fibrous fabrics, and some are partially dissolved (0.22–1.0 mm). Rare skeletal allochems include archaeocyaths, hyoliths, and trilobites. Micro-fracture sets, calcite veins and stylobrecciated features are also present.

Allochems of Microfacies 8 (peloid-ooid packstones) are entrained within a micritic matrix, which differs from the typical calcitic spar cements associated with most shallow-water high-energy ooid shoal

complexes (Markello and Read, 1981; Flügel, 2004; Bádenas and Aurell, 2010). Heterogenous composition of peloidal aggregates and sheets of quartz-enriched laminae within peloidal packstones provide evidence for fine-scale event beds and transportation (Fig. 8E). There is little evidence of internal graded bedding, though sharp erosional contacts suggest a setting prone to intermittent high-energy events (Fig. 8C).

Microfacies 9 is deposited recurrently throughout FS5 and FS6. It is characterised by packed, fine-grained, predominantly peloidal carbonates with sand-sized sub-rounded quartz entrained in a micritic matrix. Peloids are ovoid to circular, (average 0.17 mm, n=30). Matrix-supported peloidal fabrics occur as non-graded, moderately well-sorted fabrics with occasional thin quartz enriched, muddy laminae (Fig. 8D). Skeletal allochems include rare broken trilobite fragments, spicules and other indeterminate forms. A single horizon (MOG/905.4, Fig. 7F) contains rare isotropic pyrite cubes dispersed throughout, some with dissolution edges. Aggregate grains are also present in low abundance.

4.6. Facies Sequence 6 (FS6): Mernmerna Formation to Nepabunna Siltstone Member

Facies Sequence 6 is interpreted as a lower-energy deposit, accumulated on a low-gradient outer-shelf below storm wave base, with occasional event beds derived from turbidites and traction currents. This 181.4 m-thick succession features intraclastic packstones, lime mudstones, micritic sandstones, and dense spiculitic lime mudstones interbedded with peloidal packstones. The presence of a dense spiculite accords with a deeper outer-shelf setting (Thomson and Thomasson, 1969) which has previously been described for contemporaneous outcrops of the Mernmerna Formation (Third Plain Creek Member) in the Bunkers Range (Brock and Paterson, 2004, p. 136). Facies Sequence 6 includes Microfacies 7 and Microfacies 9 (described above), in addition to Microfacies 10 (intraclastic packstone, 1% of the section, Figs. 2, 8G), Microfacies 11 (micritic sandstone, 3% of section, Figs. 2, 8H) and Microfacies 12 (spiculitic lime mudstone, 10.5% of the section, Figs. 2. 8I-J). Intraclastic packstones at MOG/690 with sub-angular, poorly graded, mud-supported rip-up clasts are similarly associated with a high-energy event (tempestite). Intraclasts often contain abundant allochthonous shelly debris likely derived from semi-lithified facies shoreward of the shelf.

Microfacies 10 is characterised by heterogenous fabrics with subangular rip-up clasts (1.7–24.4 mm) entrained within a grey micritic matrix. Intraclasts are loosely packed and randomly orientated. Composition of intraclasts ranges from peloidal micrites to matrix supported skeletal wackestones dominated by archaeocyath fragments. Umbrella voids formed below intraclasts are filled by sparry calcite.

Microfacies 11 is characterised by fine, sand-sized (0.09–0.1 mm), angular to sub-rounded quartz grains and rare peloids within a micritic matrix. Pervasive iron staining obscures carbonate grains and secondary calcitic void infills disrupt fabric. Fossils are rare.

Spiculitic lime mudstones of Microfacies 12 occur at two separate intervals in FS6 from 799 to 842 m true thickness and from 959 to 981 m true thickness (Fig. 2) above the base of the section. This microfacies can be distinguished by the abundant spicules entrained within a micritic matrix. Spicules are weakly packed and orientated parallel to bedding (Fig. 8I–J). Fine sand-sized quartz grains are sparsely dispersed throughout. Rare coarse-grained irregular beds with indeterminate steinkerns, angular sand-sized quartz grains and peloids are affected by minor soft sediment deformation.

5. SSF stratigraphic distribution, palaeoenvironment, and bathymetric gradient—nMDS analyses

The nMDS ordination of the filtered abundance data converged on a solution after 20 iterations with a stress value of 0.109. The ordination of presence/absence data produced highly similar results with a stress value of 0.091. Pearson correlation coefficients of species and horizon

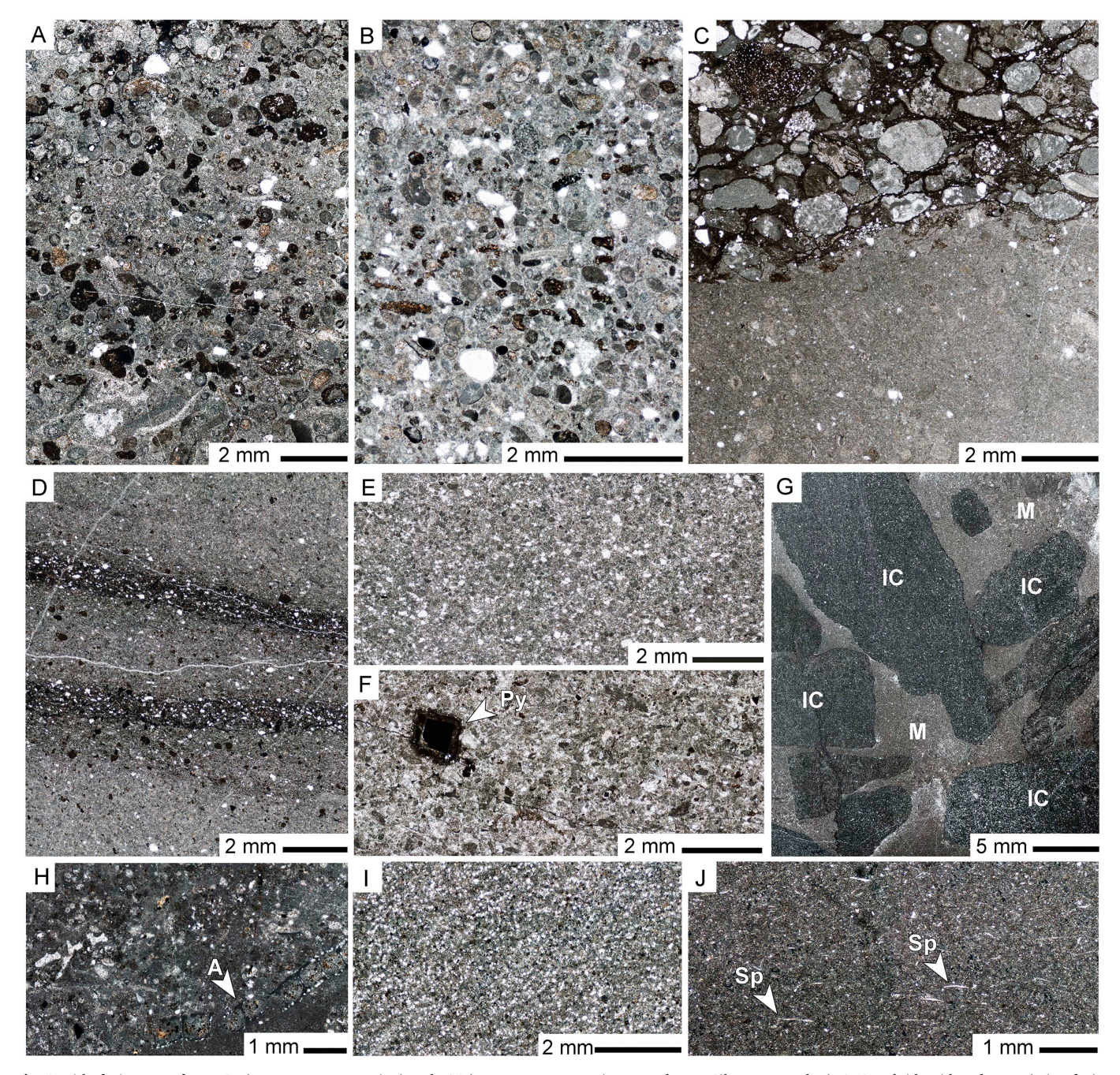


Fig. 8. Lithofacies types from FS5 (Mernmerna Formation) and FS6 (Mernmerna Formation, Nepabunna Siltstone Member). A–C. Peloid-ooid packstone (Microfacies 8). A. MOG/520.3. B. MOG/538.5. C. MOG/530.2. D–F. Peloidal packstone (Microfacies 9). D. MOG/640. E. MOG/667.4. F. MOG/905.4. G–H. Intraclastic packstone (Microfacies 10), MOG/690. I. Micritic sandstone (Microfacies 11), MOG/741.3. Spiculitic lime mudstone (Microfacies 12), MOG/818. Abbreviations: Py = pyrite, IC = intraclast, M = micrite, Sp = siliceous spicule, A = archaeocyath.

Table 1Pearson correlation analyses comparing nMDS ordination scores of the filtered abundance data and the filtered presence/absence data.

	nMDS1	nMDS2
Species	$R = 0.97 p \le 2.2e^{-16}$	R = 0.81 $p = 5.0e^{-10}$
Horizons	$R = 0.99$ $p \le 2.2e^{-16}$	$R = 0.88$ $p = 4.5e^{-15}$

nMDS1 and nMDS2 scores were consistently highly positive and statistically significant (Table 1).

The facies sequences can be separated into six corresponding

depositional settings, including semi-restricted shelf-lagoon (FS1), open inner-shelf (FS2), inner-shelf shoaling complex (FS3), mid-shelf (FS4), mid-outer shelf (FS5) and outer-shelf (FS6) (Fig. 2). This bathymetric gradient is reflected in the results of the nMDS ordination. nMDS1 scores of sampled horizons are negatively related to facies sequence values, which reflects the control of the first nMDS (nMDS1) axis by a bathymetric gradient (Fig. 9A). Facies sequences 1 and 2, the shallowest facies, generally correspond to positive nMDS1 values and FS5 and FS6, the deepest facies, correspond to negative nMDS1 values. nMDS2 values do not seem to correspond to this depth gradient.

As nMDS1 scores for samples can be used as a proxy for position along a depth gradient, we constructed a relative sea level curve based on the occurrence of fossils that is independent from that constructed

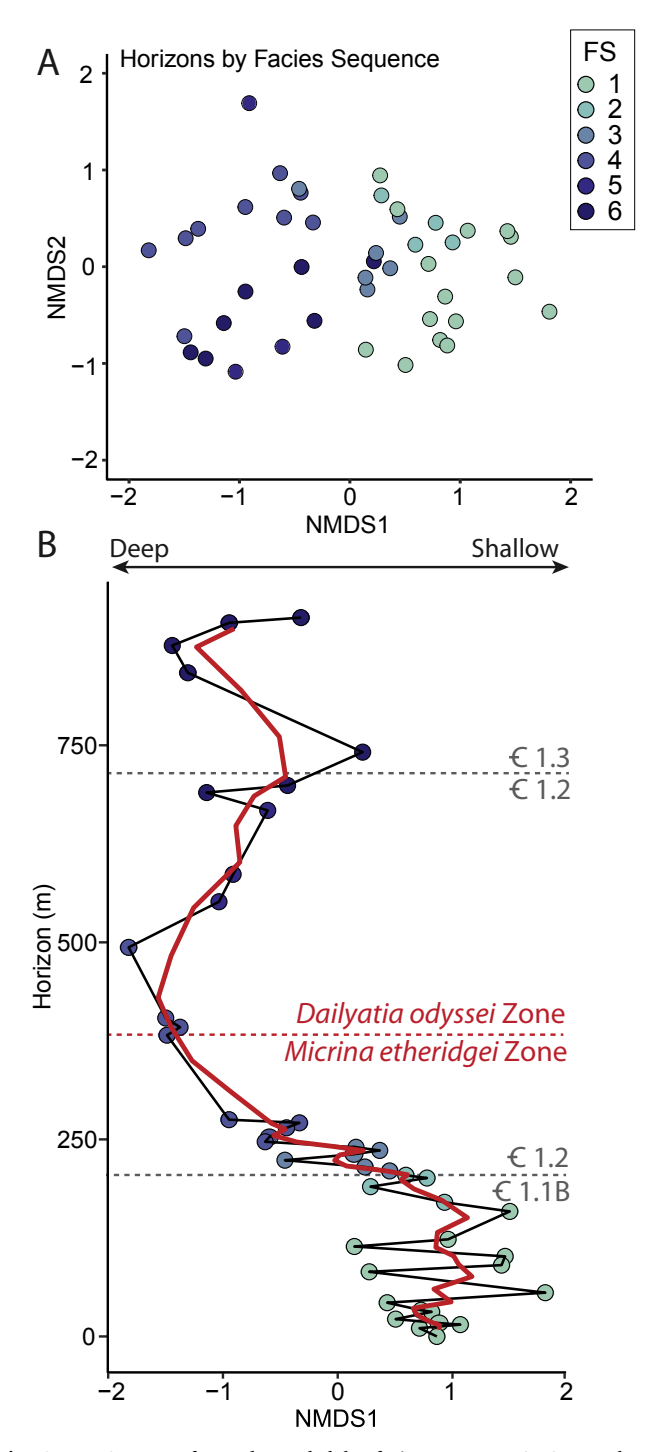
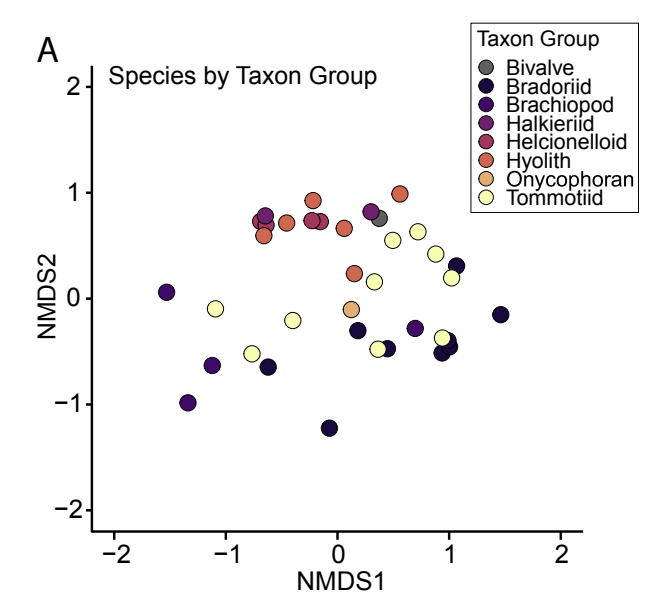


Fig. 9. nMDS sores of samples coded by facies sequence A. Scatterplot of sample nMDS1 and nMDS2 scores. B. Stratigraphic distribution of sample nMDS1 scores. The red line is the three-point moving average. (For interpretation of the references to colour in this figure legend, the reader is referred to the web version of this article.)

from sedimentological and stratigraphic proxies (Fig. 9B; see Miller et al., 2001; Scarponi and Kowalewski, 2004; Huntley et al., 2014; Wittmer et al., 2014; Scarponi et al., 2017 for similar analyses). Samples with positive scores on axis 1 are dominated by a diverse faunal assemblage with taxa characteristic of shallower-water facies (e.g. tommotiids, mollusc and bradoriids), and those with negative scores are predominantly low diversity assemblages with taxa characteristic of deeper-water facies (e.g. brachiopods). Overall we interpret four transgressive/regressive events recorded in this stratigraphic interval



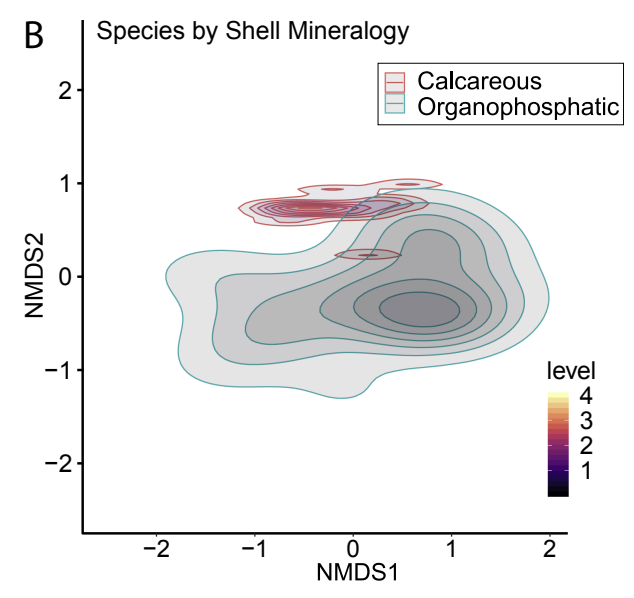
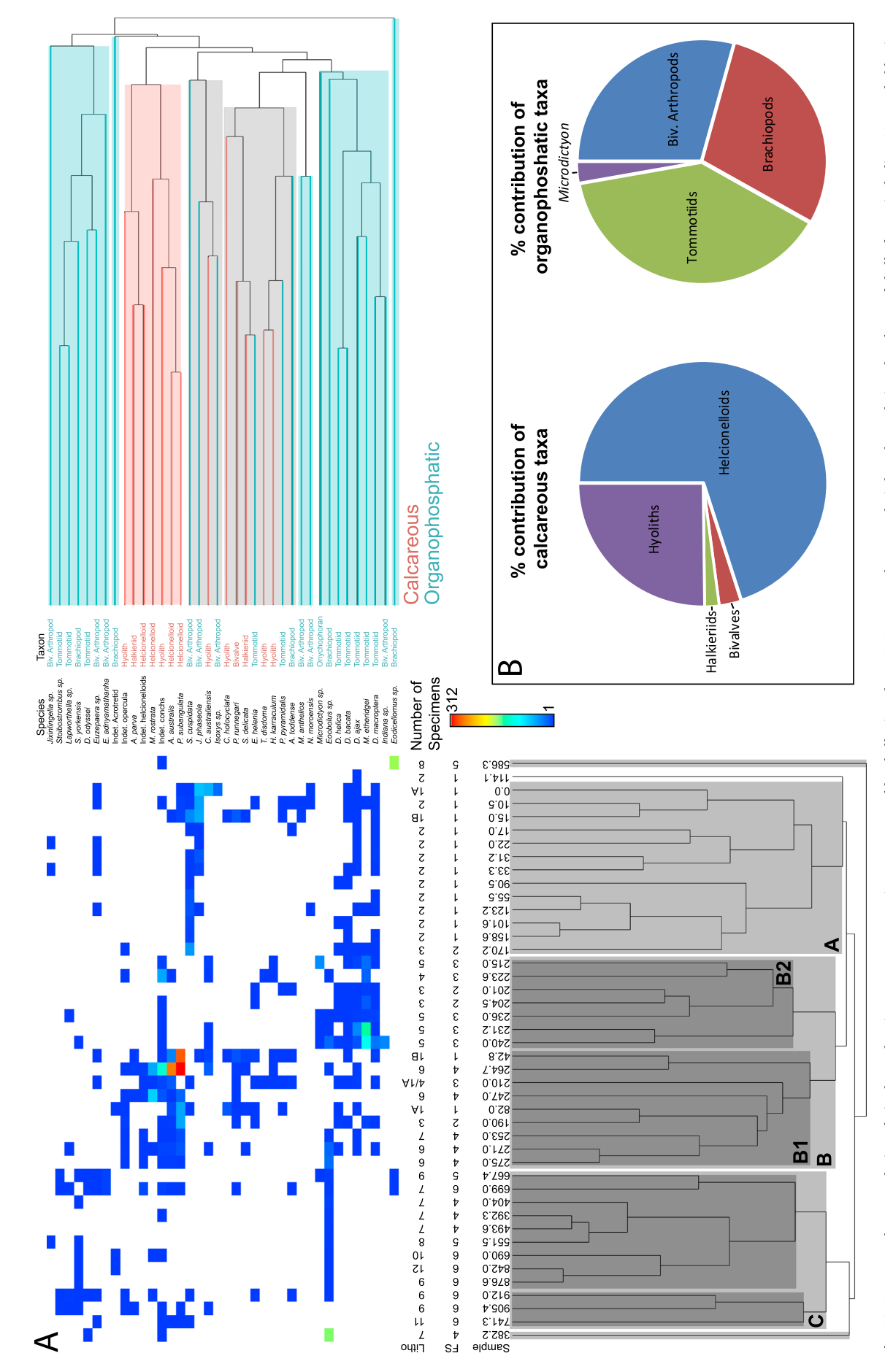


Fig. 10. nMDS sores of species coded by higher taxonomic group and shell mineralogy. A. Scatterplot of nMDS1 and nMDS2 scores for individual species colour coded by higher taxonomic group. B. Two-dimensional kernel density plots of nMDS1 and nMDS2 scores of species colour coded by shell mineralogy. Pink contours indicate calcareous taxa and turquoise contours indicate organophosphatic taxa. (For interpretation of the references to colour in this figure legend, the reader is referred to the web version of this article.)

that can be calibrated with facies sequence sets described by Gravestock and Cowley (1995) and modified by Zang et al. (2004). The temporal trend of the nMDS scores shows water depth remained relatively low throughout the deposition of FS1 and FS2, approximating highstand sequence set \in 1.1B, with minor transgressive and regressive pulses within the first \sim 230 m of the section (Fig. 9B). A major transgression took place between 230 and 250 m above the base of the section which corresponds approximately with transition from sequence \in 1.1B to \in 1.2. This is temporally corroborated by the transition from *M. etheridgei* Zone to *D. odyssei* Zone (MOG/382.2) in overlying strata, which appears conformable in the Arrowie Syncline (Betts et al., 2017). A deepening trend dominates the rest of the section, with a minor regressive phase from 400 to 700 m above the base of the section. At approximately 700 m there is another short transgressive phase marking the transition from sequence \in 1.2 to \in 1.3 (Fig. 9B).



phosphatic). The heat map colours indicate the relative abundance. B. Pie charts of the relative contributions of taxonomic groups to organophosphatic and calcareous portions of the total skeletal elements recovered from the MOG section. (For interpretation of the references to colour in this figure legend, the reader is referred to the web version of this article.) Fig. 11. Two-way cluster analysis and pie charts showing percentage constituents separated by shell mineralogy. A. Two-way cluster analysis based on relative abundance of shelly fauna, including 44 sampled horizons and 38 taxa. The dendrogram on the x-axis shows Facies Sequence and lithological groupings, and the dendrogram on the y-axis groups shelly fossil species by shell mineralogy (red = calcareous; blue = organo-

nMDS scores of samples by taxonomic group are not evenly distributed across the ordination space (Fig. 10A). Bivalved arthropods (i.e. bradoriids and *Isoxys* sp.), brachiopods, and tommotiids are broadly distributed across nMDS axis 1. Bivalved arthropods and brachiopods also span a broad range across nMDS2. Hyoliths and molluscs (inc. helcionelloids, bivalves and halkieriids) bracket -1 to +1 nMDS1 scores, but are restricted to positive nMDS2 scores (0 to 1). Similarly, species are not distributed evenly across the ordination space based upon shelly mineralogy (Fig. 10B). Organophosphatic fossils are distributed broadly across the nMDS1 axis, whilst calcareous taxa are restricted to the lower central quadrant of the scatterplot and separated into three sub-groups.

6. SSF distribution and lithofacies associations—two-way cluster analysis

The distribution and abundance of SSFs in response to changes in bathymetric gradient over the course of the MOG section are shown by a two-way cluster analysis (Fig. 11A). On the x axis, samples output three main clusters (A–C) and two outliers. The outliers include two phosphatic brachiopod species which appear in exceptional abundance in certain horizons, including *Eodicellomus elkaniiformis* Holmer & Ushatinskaya in Gravestock et al., 2001 in MOG/586.3, and *Eoobolus* sp. in MOG/382.2 (Fig. 11A). Cluster A is controlled mostly by facies sequence, with bradoriids and tommotiids occurring throughout FS1 and FS2.

The remaining two clusters (B and C) reveal several sub-clusters that are best explained by lithofacies, in particular, sub-clusters B1 and B2, which host the majority of the fauna (Fig. 11A). In sub-cluster B1 taxa are mostly associated with event deposits such as tempestites (Microfacies 6), lithologies related to low sedimentation rates (Microfacies 1A and 1B). Calcareous taxa dominate these samples, though there is a high degree of interspecific variation with regards to community composition. Together, these phosphatic firmgrounds (Microfacies 1A). incipient hardgrounds (Microfacies 1B) and trilobitic wackestones (Microfacies 6), make up just 7.7% of the section in thickness but preserve 86% of the calcareous component. In the phosphatic lithologies (Microfacies 1A and B), P. subangulata and A. australis dominate the fauna at horizons MOG/42.8 and MOG/82.0 (Fig. 11A), whereas in the trilobitic wackestones (particularly MOG/247 and MOG/264.7) both helcionelloids and hyoliths are major components. Helcionelloids including P. subangulata, A. australis and Davidonia rostrata (Zhou and Xiao, 1984) along with hyolith conchs are very abundant in Microfacies 6, but are rare in the interbedded lime mudstones of Microfacies 7 (Fig. 11A). Hyolith distribution suggests they occurred in a wider range of facies compared to other calcareous taxa (Fig. 11A). In sub-cluster B2, lithofacies are predominantly associated with archaeocyathid talus and bioclastic deposits shed from nearby biohermal facies. Organophosphatic tommotiids are the dominant taxa in this group, in particular Micrina etheridgei and species of the genus Dailyatia.

Samples grouped in cluster C contained rarer taxa or assemblages in low abundance. In general, these facies have been excessively reworked (Microfacies 9) or are representative of deposition in deeper water environments.

On the y axis, species groupings are controlled primarily by shell mineralogy, and hence, preservational mode (Fig. 11A). Most calcareous taxa (highlighted in red), group together in one cluster. Notable exceptions include *P. runnegari*, *Sinosachites delicata* (Jell, 1981), *Cupitheca holocyclata* Bengtson in Bengtson et al., 1990 and *Conotheca australiensis* Bengtson in Bengtson et al., 1990, which co-occur in phosphatic hardground horizons that fall outside of the main cluster. The remaining hyolith taxa, *Triplicatella disdoma* Conway Morris in Bengtson et al., 1990 and *Hyptiotheca karraculum* Bengtson in Bengtson et al., 1990, are rare but also exhibit some facies dependence and overlap with sub-cluster B on the x axis. Organophosphatic taxa (highlighted in blue) form two large clusters, one small cluster

(including bradoriid taxa *Neokunmingella moroensis* Betts et al., 2014 and *Mongolitubulus anthelios* Betts et al., 2014) and two outliers (*E. elkaniiformis* and Acrotretid indet.).

Helcionelloids are the most abundant skeletal element recovered from the MOG section, constituting 70% of the total primarily calcareous components (Fig. 11B). Asymmetrically coiled steinkerns of P. subangulata occur in much higher abundance relative to planispiral forms (e.g. D. rostrata and Anabarella australis Runnegar in Bengtson et al., 1990), though they share similar stratigraphic distributions and facies sequence associations (Figs. 3 and 11B). The next most abundant taxa are hyoliths at 25% (Fig. 11B), preserved by phosphate or silica replacement, or rarely with phosphate coatings that preserve external ornament. The vast majority are represented as character-poor phosphatic steinkerns, with variable retention of fine details, often precluding confident taxonomic assignment. Even rarer are hyolith opercula, which when present are almost always preserved as phosphatic coatings, and occasionally silicified replacement. The remaining minor constituents of the calcareous fauna include bivalve species, P. runnegari and halkieriid sclerites (3% and 2% respectively; Fig. 11B). Pojetaia runnegari exhibits a similar stratigraphic distribution to that of helcionelloids (Fig. 3), and specimens are preserved predominantly as steinkerns enveloped by phosphatic coatings. Sclerites of halkieriid taxa S. delicata and Australohalkieria parva (Conway Morris in Bengtson et al., 1990) are also preserved as rare steinkerns with partial phosphatic coatings (Fig. 3).

Among the organophosphatic taxa, tommotiids are most abundant (39%, Fig. 11B), with two dominant genera—*Micrina* and *Dailyatia* of the ten species identified in the MOG section. Brachiopods and bradoriids make up \sim 29% respectively (Fig. 11B). *Microdictyon* sclerites make up only 3%.

7. Discussion

7.1. Major controls on SSF distribution, abundance, and preservation potential in the MOG section

The stratigraphic distribution of species along the MOG section exhibits a clear response to a bathymetric gradient. Multivariate analyses show SSF communities in each facies sequence can be separated into shallower-water assemblages in association with positive nMDS1 scores, to deeper-water assemblages with negative scores. Ordinations coded by taxonomic grouping, and similarly by shell mineralogy, are affected less by bathymetry, but still provide information on the environmental distribution of taxa. For instance, organophosphatic taxa are broadly distributed in the ordination space, suggesting they have a wider environmental distribution. By contrast, calcareous taxa are more restricted, suggesting there are environmental, taphonomic and/or sampling biases further limiting their occurrence.

Patterns in the relative abundance of taxa across the section, as revealed by the two-way cluster analysis, further underpin the influence of a bathymetric gradient and subsequent taphonomic overprint on the distribution of taxa. The majority of SSF are found in association with shallow-water environments, principally protected shelf/lagoonal (FS1), inner-shelf shoals (FS3), and mid-shelf environments (FS4). Notably, this method offers additional means to tease out species-level distribution patterns and underlying taphonomic controls. This is most evident in the apparent stratigraphic distribution of the calcareous taxa, which cluster together in association with specific lithofacies (Fig. 11A). As such, the calcareous component of SSF in the MOG section exhibit what may be interpreted as a strong facies dependence. However this apparent lithofacies association is more likely to represent taphonomic overprint due to the preservational constraints imposed on calcareous taxa as a result of their shell mineralogy (i.e. recrystallization and dissolution), rather than facies control imposed on the organisms themselves. Hence, the stratigraphic distribution of calcareous taxa, as revealed by acid residues, is controlled by depositional

conditions conducive to their preservation as phosphatic steinkerns, coatings, or replaced shell. These deposits represent important taphofacies for the preservation of calcareous shelly fossils.

7.2. Depositional regimes conducive to phosphogenesis and enhanced preservation potential

In the MOG section, the best preserved and most abundant phosphatic remains of calcareous groups occur in firmgrounds and incipient hardgrounds (Microfacies 1A, B), bioclastic floatstone (Microfacies 4), and trilobitic wackestone (Microfacies 6). These lithofacies encompass specific hydrodynamically controlled depositional regimes in which sediment accumulation, winnowing, and reworking operate to produce conditions conducive to phosphogenesis, and hence, enhanced preservation potential of small shelly fossils.

Phosphatic condensed horizons (sensu Föllmi, 2016), including the firmground and incipient hardgrounds present in FS1 have irregular omission surfaces, discontinuous internal phosphatic laminae, and reworked clasts (Figs. 4A–D, 5, 6), and bear all the hallmarks of repeated phases of current-induced winnowing, erosion, phosphogenesis, and nondeposition. The interplay of these processes in the MOG section is comparable to models developed for the formation of hardground facies (summarised by Föllmi, 2016) in much younger deposits, such as the middle Miocene Monterey Formation in the Santa Barbara Basin (1991), and the Oligocene-Miocene successions on Malta and southeastern Sicily, Italy (Föllmi et al., 2008).

The internal fabrics of Microfacies 1A and 1B are also closely comparable with the few previously documented early Cambrian hardgrounds, which similarly include thin phosphatic laminae, lag deposits, and phosphatic hardgrounds (Alexander and Gravestock, 1990; Dzik, 1991; Clausen and Álvaro, 2007). Assemblages dominated by calcareous taxa are commonly preserved in association with these facies. For instance, hyolith packstones occur immediately above hardground surfaces in Facies C of the lower Cambrian Sellick Hill Formation, eastern Stansbury Basin (Alexander and Gravestock, 1990, fig. 9F). Molluscs are also prevalent in lag deposits associated with phosphatic discontinuity surfaces in Tommotian (Cambrian Stage 2) strata in Yutia, Siberia (Dzik, 1991, fig. 6C). Skeletal material in these types of deposits has been transported and deposited as time-averaged assemblages within the topographic lows of phosphatic omission surfaces.

Petrographic analysis reveals that phosphatic steinkerns (Fig. 6C, D [P]), coatings or rims (Fig. 6C–E [P]), and replacements occur in higher abundance when entrained in the micritic matrix between thinner interstitial layers of phosphatic surfaces (Fig. 4C, D). This indicates that sources of phosphate associated with the enriched precipitation of phosphorus in the upper crust of the omission surfaces may also be linked to both phosphatization and localised phosphogenesis of shelly fossils. This is supported by an apparent absence of phosphatic steinkerns in underlying wackestones and mudstones, wherein calcitic shells are recrystallized and occasionally infilled by blocky spar. The origin of this phosphorous is unknown. Enriched phosphorus in the upper crust of the laminae is suggestive of an external source (rather than organic sources [decay] within the sediment), however upwelling seems unlikely for the marine lagoonal setting proposed herein (Föllmi et al., 2005).

Moderate to high-energy deposits forming shoal talus and bioclastic lenses within the inner-shelf represent a second important taphonomic filter for select calcareous taxa. For instance hyoliths whose aragonitic shells (Kouchinsky, 2000; Li et al., 2018) are either replaced, coated, or preserved as phosphatic steinkerns occur in abundance within the bioclastic floatstones found adjacent to the archaeocyathid rudstones (Figs. 3, 11). These high-energy inner-shelf environments reduce the likelihood of dissolution of aragonitic shells (Runnegar et al., 1975; Kouchinsky, 2000), by removing organics and inhibiting microbial decay (Cherns et al., 2011). Intermittent periods of phosphogenesis are also apparent within this depositional setting as evidenced by thin phosphate-rich laminae within the microfabric of MOG/210

(Fig. 5G-H).

Different taphonomic processes operate in mid-shelf settings where current action in conjunction with event beds (traction currents and turbidites) becomes increasingly frequent. Regular winnowing and reworking by current or wave action removes and redistributes finegrained sediment and organics (Cherns et al., 2008, 2011). These processes may be important in remobilizing phosphate-rich sediments and initiating a second, or multiple phases of phosphatization or phosphate mineralization (Föllmi, 1996; Frauhiger et al., 2018). As these higherenergy events contribute to localised changes in the redox conditions—whether by oxidizing sediments or helping to reduce them by trapping decaying organic matter—there is enhanced potential for phosphate nucleation and precipitation (Föllmi, 1996; Briggs, 2003; Creveling et al., 2014a, 2014b; Schiffbauer et al., 2014; Pruss et al., 2018). Particularly in the case of phosphatic steinkerns, the source of phosphorus is more likely associated with organic-bound phosphorous released from the decaying organism itself, or any other organics picked up during sediment reworking.

7.3. Implications for applied uses of calcareous small shelly fossil taxa

The integrated sedimentological and palaeontological data coupled with multivariate analyses along the MOG section reveal that SSF occurrences of originally calcareous taxa—helcionelloids, bivalves, hyoliths, and halkieriids—are not only affected by an environmental gradient, but also specific hydrodynamic regimes conducive to phosphogenesis and phosphatization. This explains the remarkably patchy stratigraphic distribution and abundance of calcareous taxa in the MOG section, affecting (and skewing) the biostratigraphic ranges of taxa through time.

Evaluation of the lithological samples and fossils within their original environmental context enables assessment of their utility as index fossils. Bivalved arthropods, brachiopods, and tommotiids tend to have the broadest environmental distributions making them more suitable candidates for index fossils, whereas molluscs and hyoliths are more limited in environmental distribution. Calcareous taxa occupy only a minor portion of the nMDS ordination space. This suggests that preservation of calcareous taxa is strongly related to depositional environment and preservation potential (and extraction methods), decreasing the likelihood of recovery when sampling through a stratigraphic section. This has clear implications for the application of these taxa as index fossils, and casts doubt over biostratigraphic schemes that rely primarily on such taxa. Whilst some organophosphatic taxa do seem to demonstrate a preference for certain environments (e.g. linguiform brachiopods such as E. elkaniiformis and Eoobolus sp. in the MOG section [Figs. 3, 13]), many organophosphatic fauna span the breadth of the water depth gradient, are very abundant and are likely to be more useful as index fossils in lower Cambrian stratigraphic successions.

Shelly fossil biozones defined by secondarily replaced or infilled fossils feature in many early Cambrian (Terreneuvian - Series 2) regional biostratigraphic schemes, including those from the Siberian platform (Rozanov and Missarzhevsky, 1966; Rozanov et al., 1969; Matthews and Missarzhevsky, 1975), South China (Steiner et al., 2007; Li et al., 2011; Yang et al., 2014), Mongolia (Brasier et al., 1996; Esakova and Zhegallo, 1996), West Gondwana (Devaere et al., 2013) and South Australia (Gravestock et al., 2001). This study highlights the need to critically assess lithological and taphonomic constraints on the stratigraphic distribution of shelly faunas. Caution is required when using calcareous taxa to define biozones in regional biostratigraphic schemes (Jacquet et al., 2014). For instance, Betts et al. (2016, 2017) utilise molluscs only as supplementary taxa in defining new shelly fossil biozones in the lower Cambrian of South Australia.

Identification of Cambrian calcareous taxa based primarily on phosphatic steinkerns inevitably leads to ambiguous taxonomic assignment, especially in speciose genera with simple or conservative shell morphology (e.g. *Pelagiella*, *Aldanella*, and hyolith conchs). Some

monospecific taxa with distinctive shell morphology are readily taxonomically identified based on complete phosphatic steinkerns, for example, Watsonella crosbyi Grabau, 1900. However, occurrences of these taxa are still strongly taphonomically-controlled which may obscure true first occurrence data in a stratigraphic succession (see also Landing et al., 2013, p. 145). Recent suggestions to define the base of early Cambrian Terreneuvian Series, Stage 2 (Li et al., 2011; Peng et al., 2012; Parkhaev, 2014) using the first occurrence of Watsonella crosbyi should also include detailed microfacies analyses of stratigraphic strata above and below the nominate boundary to determine depositional regimes, amount of phosphatic accumulation and presence or absence of original, replaced or infilled shells of the nominate mollusc taxon.

8. Conclusions

Small, calcareous fossils are normally recovered (in small numbers) via "crack out" techniques, usually reserved for macro-scale faunas (e.g. trilobites), and calcareous forms not preserved by phosphatization or phosphogenesis are destroyed in the acid digestion process. Hence, sampling bias remains a primary driver of the reported stratigraphic patterns of calcareous faunas. In the lower Cambrian MOG section, integration of microfacies analysis with microfossil residues demonstrate that reported stratigraphic distribution of the two main biomineralizing components of SSF assemblages-originally organophosphatic and calcareous skeletons—are controlled by different factors. Organophosphatic taxa are less constrained by preservational environment, and occur along the breadth of the observed bathymetric gradient across an early Cambrian marine shelf-ramp setting. However, specific taxonomic groups tend to occupy different environments, suggesting habitat preference is the main driver in their stratigraphic distribution. In contrast, calcareous fossils exhibit strong taphonomic control, and their stratigraphic distribution reflects conditions conductive to preservation rather than true stratigraphic ranges.

For calcareous taxa to be represented in insoluble acid residues, shells must have been infilled (i.e. phosphatic steinkern formation), coated, or replaced via other insoluble minerals. Phosphatic facies hosting these taxa in the studied section were identified as firmgrounds, incipient hardgrounds, bioclastic floatstones, and bioclastic lime mudstones. Hence, occurrence of calcareous shells (especially molluscan assemblages) in these facies is influenced by preservational, environmental, and depositional event processes, such as sedimentation rates, fluctuations in energy regimes, and sediment reworking and winnowing.

Whilst acid maceration techniques are ideal for recovery and taxonomic study of originally phosphatic small shelly fossils, this method has clear limitations when applied to originally calcareous groups. The process is inherently biased towards phosphatic or secondarily phosphatized remains. For calcareous taxa such as chancelloriids, archaeocyathans, molluscs, hyoliths, some brachiopods, and arthropods, this process filters out an unknown proportion of originally calcareous material. This, in conjunction with the taphofacies-dependence directly associated with preferential conditions for phosphatization and phosphate mineralization reported herein, has implications for application of calcareous taxa in regional and global biostratigraphic schemes. We recommend that, given the broad environmental distribution, enhanced preservation potential, and readily identifiable features of organophosphatic taxa, these faunas take precedence in biozonation of SSFbearing Cambrian successions. Unless the taxon is readily identifiable as monospecific and morphologically distinct, calcareous faunas are best used as supplementary taxa in establishing regional biostratigraphic schemes in the early Cambrian.

Acknowledgments

We would like to thank the Adnyamathanha people of Nepabunna, the Traditional Custodians of the Land, for allowing fieldwork and collection in the Flinders Ranges, South Australia; J. Valentine,

D. Mathieson, S. Collison, and B. Mamo, for assistance in the field; David Adams, Norman Pearson, and Timothy D. Murphy from Macquarie University GeoAnalytical for assistance and advice with EDS and XRF imaging and data; Staff in the Microscopy Unit (MQ) for assistance with SEM imaging; Steve Craven for access to polishing facilities (MQ); Nathan Daczko for use of the petrographic (Nikon Eclipse 663 50ipol) Microscope (MQ); Dave Keith for petrographic thin sectioning (University of New England); and D. Oliver (Dean Oliver Graphics) for the original drafting of Fig. 1. This work has been supported by funding from the Australian Research Council Discovery [Project # 129104251 to GAB], and Macquarie University Postgraduate Research Fund (PGRF) funds (to SMJ and MJB). JWH is supported by NSF CAREER 1650745. We are grateful to Rebecca Freeman (University of Kentucky) and one other anonymous reviewer for their constructive reviews which benefited the submitted manuscript.

Appendix A. Supplementary data

Supplementary data to this article can be found online at https:// doi.org/10.1016/j.palaeo.2019.05.022.

References

- Alexander, F.M., Gravestock, D.L., 1990, Sedimentary facies in the Sellick Hill Formation. Fleurieu Peninsula, South Australia, in: Jago, J.B., Moore, P.S. (Eds.), The Evolution of a Late Precambrian-Early Palaeozoic Rift Complex: The Adelaide Geosyncline, Geological Society of Australia, Special Publication, p. 269-289.
- Bádenas, B., Aurell, M., 2010. Facies models of a shallow-water carbonate ramp based on distribution of non-skeletal grains (Kimmeridgian, Spain). Facies 56, 89-110.
- Bengtson, S., Conway Morris, S., Cooper, B.J., Jell, P.A., Runnegar, B.N., 1990. Early Cambrian fossils from South Australia. Memoir 9 of the Association of Australasian Palaeontologists 7, 1-364.
- Betts, M.J., Topper, T.P., Valentine, J.L., Skovsted, C.B., Paterson, J.R., Brock, G.A., 2014. A new early Cambrian bradoriid (Arthropoda) assemblage from the northern Flinders Ranges, South Australia. Gondwana Res. 25, 420-437.
- Betts, M.J., Paterson, J.R., Jago, J.B., Jacquet, S.M., Skovsted, C.B., Topper, T.P., Brock, G.A., 2016. A new lower Cambrian shelly fossil biostratigraphy for South Australia. Gondwana Res. 36, 176-208.
- Betts, M.J., Paterson, J.R., Jago, J.B., Jacquet, S.M., Skovsted, C.B., Topper, T.P., Brock, G.A., 2017. Global correlation of the early Cambrian of South Australia: shelly fauna of the Dailyatia odyssei Zone. Gondwana Res. 46, 240-279.
- Betts, M.J., Paterson, J.R., Jacquet, S.M., Andrew, A.S., Hall, P.A., Jago, J.B., Jagodzinski, E.A., Preiss, W.V., Crowley, J.L., Brougham, T., 2018. Early Cambrian chronostratigraphy and geochronology of South Australia. Earth Sci. Rev. 185, 498-543.
- Brasier, M., 1990. Phosphogenic events and skeletal preservation across the Precambrian-Cambrian boundary interval. Geol. Soc. Lond., Spec. Publ. 52, 289-303.
- Brasier, M., Shields, G., Kuleshov, V., Zhegallo, E., 1996. Integrated chemo-and biostratigraphic calibration of early animal evolution; Neoproterozoic-early Cambrian of southwest Mongolia. Geol. Mag. 133, 445-485.
- Briggs, D.E., 2003. The Role of Decay and Mineralization in the Preservation of Softbodied Fossils. Annual Review of Earth and Planetary Sciences 31. pp. 275-301.
- Brock, G.A., Paterson, J.R., 2004. A New Species of Tannuella (Helcionellida, Mollusca) From the Early Cambrian of South Australia. Association of Australasian Palaeontologists Memoir. vol. 30. pp. 135–143. Cherns, L., Wheeley, J.R., Wright, V.P., 2008. Taphonomic windows and molluscan
- preservation. Palaeogeogr. Palaeoclimatol. Palaeoecol. 270, 220-229.
- Cherns, L., Wheeley, J.R., Wright, V.P., 2011. Taphonomic bias in shelly faunas through time: early aragonitic dissolution and its implications for the fossil record. In: Allison, P.A., Bottjer, D.J. (Eds.), Taphonomy: Process and Bias Through Time. Springer Netherlands, Dordrecht, pp. 79-105.
- Christ, N., Immenhauser, A., Wood, R.A., Darwich, K., Niedermayr, A., 2015. Petrography and environmental controls on the formation of Phanerozoic marine carbonate hardgrounds. Earth Sci. Rev. 151, 176-226.
- Clarke, J., 1986a. Stratigraphy and sedimentology of the upper part of the Wilkawillina Limestone, Wilkawillina Gorge, Flinders Ranges. Geological Survey of South Australia 100, 2-7.
- Clarke, J., 1986b. Subdivision of the Early Cambrian Parara Limestone at Wilkawillina Gorge, Flinders Ranges. Quarterly Geological Notes. Geological Survey of South Australia 99, 2-7.
- Clarke, J., 1986c. Subdivision of the lower part of the Wilkawillina Limestone, eastern Flinders Ranges. Quarterly Geological Notes. Geological Survey of South Australia
- Clarke, J.D.A., 1990a. Platform carbonate deposition and diagenesis, Woodendinna Dolomite and lower Wilkawillina Limestone (Early Cambrian), Wilkawillina Gorge, South Australia. Geological Society of Australia Special Publication 16, 247-268.
- Clarke, J.D.A., 1990b. Slope Facies Deposition and Diagenesis of the Early Cambrian Parara Limestone, Wilkawillina Gorge, South Australia, The Evolution of a Late Precambrian-Early Palaeozoic Rift Complex, the Adeliade Geosyncline. vol. 16. pp
- Clausen, S., Álvaro, J.J., 2007. Lower Cambrian shelled phosphorites from the northern Montagne Noire, France. Geol. Soc. Lond., Spec. Publ. 275, 17-28.
- Creveling, J.R., Johnston, D.T., Poulton, S.W., Kotrc, B., März, C., Schrag, D.P., Knoll,

- A.H., 2014a. Phosphorus sources for phosphatic Cambrian carbonates. Geol. Soc. Am. Bull. 126, 145-163.
- Creveling, J.R., Knoll, A.H., Johnston, D.T., 2014b. Taphonomy of Cambrian phosphatic small shelly fossils. Palaios 29, 295-308.
- Dattilo, B.F., Freeman, R.I., Peters, W.S., Heimbrock, W.P., Deline, B., Martin, A.J., Kallmeyer, J.W., Reeder, J., Argast, A., 2016. Giants among micromorphs: were Cincinnatian (Ordovician, Katian) small shelly phosphatic faunas dwarfed? Palaios
- Devaere, L., Clausen, S., Steiner, M., Álvaro, J.J., Vachard, D., 2013. Chronostratigraphic and palaeogeographic significance of an early Cambrian microfauna from the Heraultia Limestone, northern Montagne Noire, France. Palaeontol. Electron. 16,
- Dzik, J., 1991. Is fossil evidence consistent with traditional views of the early metazoan phylogeny. In: Simonetta, A.M., Conway Morris, S. (Eds.), The Early Evolution of Metazoa and the Significance of Problematic Taxa. Cambridge. Cambridge University
- Press, pp. 47–58.

 Dzik, J., 1994. Evolution of 'small shelly fossils' assemblages of the early Paleozoic. Acta Palaeontol. Pol. 39, 247-313.
- Esakova, N.V., Zhegallo, E.A., 1996. Biostratigraphy and fauna of Lower Cambrian of Mongolia. Sovmestnaya Rossiisko-Mongol'skaya. Paleontologicheskaya Ekspeditsiya Trudy 46, 1-214.
- Flügel, E., 2004. Microfacies of Carbonate Rocks: Analysis, Interpretation and Application. Springer.
- Föllmi, K.B., 1996. The phosphorus cycle, phosphogenesis and marine phosphate-rich deposits. Earth Sci. Rev. 40, 55-124.
- Föllmi, K.B., 2016. Sedimentary condensation. Earth Sci. Rev. 152, 143–180.
- Föllmi, K.B., Badertscher, C., de Kaenel, E., Stille, P., John, C.M., Adatte, T., Steinmann, P., 2005. Phosphogenesis and organic-carbon preservation in the Miocene Monterey Formation at Naples Beach, California—the Monterey hypothesis revisited. GSA Bull. 117, 589–619.
- Föllmi, K., Gertsch, B., Renevey, J.P., De Kaenel, E., Stille, P., 2008. Stratigraphy and sedimentology of phosphate-rich sediments in Malta and south-eastern Sicily (latest Oligocene to early Late Miocene). Sedimentology 55, 1029–1051.

 Frauhiger, M.J., Dattilo, B.F., Freeman, R.L., Peters, W.S., 2018. Upper Middle Triassic
- "Small Shellies" From the Kleine Terrebratelbank of the Muschelkalk, Bavaria, Germany: The Role of Attention Bias in Underestimating the Distribution of Phosphatic Microsteinkerns, Geological Society of America Abstracts With Programs.
- Fürsich, F., Oschmann, W., 1993. Shell beds as tools in basin analysis: the Jurassic of Kachchh, western India. J. Geol. Soc. 150, 169–185.
- Gravestock, D.I., Cowley, W.M., 1995. Arrowie Basin. The geology of South Australia In: Drexel, J.F., Priess, W.V. (Eds.), The Phanerozoic. Mines and Energy, South Australia. vol. 2. pp. 20-31.
- Gravestock, D.I., Alexander, E.M., Demidenko, Y.E., Esakova, N.V., Holmer, L.E., Jago, J.B., Lin, T.-R., Melnikova, L.M., Parkhaev, P.Y., Rozanov, A.Y., Ushatinskaya, G.T., Zang, W.-L., Zhegallo, E.A., Zhuravlev, A.Y., 2001. The Cambrian Biostratigraphy of the Stansbury Basin. (South Australia. Transactions of the Palaeontological Institute).
- Haslett, P.G., 1975. The Woodendinna Dolomite and Wirrapowie Limestone-two new Lower Cambrian formations, Flinders Ranges, South Australia. Trans. R. Soc. S. Aust. 99, 211-220.
- Hillgaertner, H., 1998. Discontinuity surfaces on a shallow-marine carbonate platform (Berriasian, Valanginian, France and Switzerland). J. Sediment. Res. 68, 1093-1108.
- Holmer, L.E., Skovsted, C.B., Brock, G.A., Valentine, J.L., Paterson, J.R., 2008. The Early Cambrian tommotiid Micrina, a sessile bivalved stem group brachiopod. Biol. Lett. 4, 724-728.
- Huntley, J.W., Fürsich, F.T., Alberti, M., Hethke, M., Liu, C., 2014. A complete Holocene record of trematode-bivalve infection and implications for the response of parasitism to climate change. Proc. Natl. Acad. Sci. 111, 18150-18155.
- Jacquet, S.M., Brock, G.A., 2016. Lower Cambrian helcionelloid macromolluscs from South Australia. Gondwana Res. 36, 333-358.
- Jacquet, S.M., Brock, G.A., Skovsted, C.B., 2014. Reassessment of the Lower Cambrian Molluscan Biostratigraphy From South Australia., International Subcommission of Cambrian Stratigraphy. Program and Abstracts, Morocco, p. 21.
- James, N.P., Gravestock, D.I., 1990. Lower Cambrian shelf and shelf margin buildups, Flinders Ranges, South Australia. Sedimentology 37, 455-480.
- Jell, P.A., 1981. Thambetolepis delicata gen. et sp. nov., an enigmatic fossil from the Early Cambrian of South Australia. Alcheringa: An Australasian Journal of Palaeontology 5, 85-93.
- Jeppsson, L., Anehus, R., Fredholm, D., 1999. The optimal acetate buffered acetic acid technique for extracting phosphatic fossils. J. Paleontol. 73, 964–972.
- Kouchinsky, A.V., 2000. Skeletal microstructures of hyoliths from the Early Cambrian of Siberia. Alcheringa: An Australasian Journal of Palaeontology 24, 65-81.
- Kouchinsky, A., Bengtson, S., Clausen, S., Vendrasco, M.J., 2015. An Early Cambrian fauna of skeletal fossils from the Emyaksin Formation, Northern Siberia. Acta Palaeontol. Pol. 60, 421-512.
- Landing, E., 1988. Lower Cambrian of eastern Massachusetts: stratigraphy and small shelly fossils. J. Paleontol. 62, 661–695.
 Landing, E., Bartowski, K.E., 1996. Oldest shelly fossils from the Taconic allochthon and
- late Early Cambrian sea-levels in eastern Laurentia. J. Paleontol. 70, 741–761.
- Landing, E., Myrow, P., Benus, A.P., Narbonne, G.M., 1989. The Placentian Series: aparance of the oldest skeletalized faunas in southeastern Newfoundland. J. Paleontol. 63, 739–769.
- Landing, E., Geyer, G., Brasier, M.D., Bowring, S.A., 2013. Cambrian evolutionary radiation: context, correlation, and chronostratigraphy—overcoming deficiencies of the first appearance datum (FAD) concept. Earth Sci. Rev. 123, 133–172.
- Li, G., Zhao, X., Gubanov, A.P., Zhu, M., Na, L., 2011. Early Cambrian mollusc Watsonella crosbyi: a potential GSSP index fossil for the base of the Cambrian stage 2. Acta Geologica Sinica - English Edition 85, 309-319.

- Li, L., Zhang, X., Skovsted, C.B., Yun, H., Pan, B., Li, G., 2018. Homologous shell microstructures in Cambrian hyoliths and molluscs. Palaeontology. 1-18. https://doi. org/10.1111/pala.12406.
- Markello, J., Read, J., 1981, Carbonate ramp-to-deeper shale shelf transitions of an Upper Cambrian intrashelf basin, Nolichucky Formation, Southwest Virginia Appalachians. Sedimentology 28, 573-597.
- Martí Mus, M., Palacios, T., Jensen, S., 2008. Size of the earliest mollusks: did small helcionellids grow to become large adults? Geology 36, 175-178.
- Matthews, S.C., Missarzhevsky, V.V., 1975. Small shelly fossils of late Precambrian and
- early Cambrian age: a review of recent work. J. Geol. Soc. Lond. 131 989–304. Miller, A.I., Holland, S.M., Meyer, D.L., Dattilo, B.F., 2001. The use of faunal gradient analysis for intraregional correlation and assessment of changes in sea-floor topography in the type Cincinnatian. The Journal of Geology 109, 603-613.
- Nordlund, U., 1989. Genesis of phosphatic hardgrounds in the Lower Ordovician of northern Öland, Sweden. GFF 111, 161-170.
- Oksanen, J., Blanchet, F.G., Friendly, M., Kindt, R., Legendre, P., McGlinn, D., Minchin, P. R., O'Hara, R.B., Simpson, G.L., Solymos, P., Stevens, M.H.H., Szoecs, E., Wagner, H., 2017. Vegan: community ecology package. R package version 2.4-4. URL:. https://CRAN.R-project.org/package=vegan.

 Palmer, T.J., Hudson, J., Wilson, M.A., 1988. Palaeoecological Evidence for Early
- Aragonite Dissolution in Ancient Calcite Seas.
- Parkhaev, P.Y., 2014. On the stratigraphy of Aldanella attleborensis-potential index species for defining the base of Cambrian Stage 2. In: IGCP Project 591 Field Workshop, pp. 102-105.
- Parkhaev, P., Demidenko, Y., 2010. Zooproblematica and mollusca from the Lower Cambrian Meishucun section (Yunnan, China) and taxonomy and systematics of the Cambrian small shelly fossils of China. Paleontol. J. 44, 883–1161.
- Peng, S., Babcock, L.E., Cooper, R.A., 2012. The Cambrian period. In: Gradstein, F.M., Ogg, J.G., Schmitz, M., Ogg, G. (Eds.), The Geologic Time Scale 2012 2-Volume Set, Volume 2. Elsevier, pp. 437-488.
- Porter, S.M., 2004. Closing the phosphatization window: testing for the influence of ta-
- phonomic megabias on the pattern of small shelly fossil decline. Palaios 19, 178–183. Pruss, S.B., Tosca, N.J., Stark, C., 2018. Small shelly fossil preservation and the role of early diagenetic redox in the early Triassic. Palaios 33, 441–450.
- Rozanov, A.Y., Missarzhevsky, V.V., 1966. Biostratigraphy and fauna of the Lower Cambrian horizons. Akademiya Nauk SSSR. Trudy Geologicheskiy Institut 148,
- Rozanov, A.Y., Missarzhevsky, V.V., Volkova, N.A., Voronova, L.G., Krylov, I.N., Keller, B.M., Korolyuk, I.K., Lendzion, K., Michniak, R., Pychova, N.G., Sidorov, A.D., 1969. The Tommotian Stage and the Cambrian lower boundary problem. Transactions of the Academy of Sciences of the USSR Nauka 206, 1-380.
- Runnegar, B., Pojeta, J., Morris, N.J., Taylor, J.D., Taylor, M.E., McClung, G., 1975. Biology of the Hyolitha. Lethaia 8, 181-191.
- Scarponi, D., Kowalewski, M., 2004. Stratigraphic paleoecology: bathymetric signatures and sequence overprint of mollusk associations from upper Quaternary sequences of the Po Plain, Italy. Geology 32, 989–992.

 Scarponi, D., Azzarone, M., Kowalewski, M., Huntley, J.W., 2017. Surges in trematode
- prevalence linked to centennial-scale flooding events in the Adriatic. Sci. Rep. 7, 5732
- Schiffbauer, J.D., Wallace, A.F., Broce, J., Xiao, S., 2014. Exceptional fossil conservation through phosphatization. Paleontol. Soc. Pap. 20, 59-82.
- Skovsted, C.B., 2006. Small shelly fossils from the basal Emigrant Formation (Cambrian, uppermost Dyeran Stage) of Split Mountain, Nevada. Can. J. Earth Sci. 43, 487-496.
- Steiner, M., Li, G., Qian, Y., Zhu, M., 2004. Lower Cambrian small shelly fossils of northern Sichuan and southern Shaanxi (China), and their biostratigraphic importance. Geobios 37, 259-275.
- Steiner, M., Li, G., Qian, Y., Zhu, M., Erdtmann, B.-D., 2007. Neoproterozoic to Early Cambrian small shelly fossil assemblages and a revised biostratigraphic correlation of the Yangtze Platform (China). Palaeogeogr. Palaeoclimatol. Palaeoecol. 254, 67-99.
- Team, R.C., 2017. R: a language and environment for statistical computing. R Foundation for Statistical Computing, Vienna, Austria. In: URL, https://www.R-project.org/. Thomas, R.D., 2005. In: Callebaut, W., Rasskin-Gutman, D. (Eds.), Hierarchical
- Integration of Modular Structures in the Evolution of Animal Skeletons. MIT Press, Cambridge, pp. 239-258 Modularity: Understanding the Development and Evolution of Complex Natural Systems.
- Thomas, R., Shearman, R.M., Stewart, G.W., 2000. Evolutionary exploitation of design options by the first animals with hard skeletons. Science 288, 1239-1242.
- Thomson, A.F., Thomasson, M.R., 1969. Shallow to deep water facies development in the Dimple Limestone (Lower Pennsylvanian), Marathon region. Texas. Society of Economic Paleontologists and Mineralogists 14, 57–78.
- Westrop, S.R., 1986. Taphonomic versus ecologic controls on taxonomic relative abundance patterns in tempestites. Lethaia 19, 123-132.
- Wittmer, J.M., Dexter, T.A., Scarponi, D., Amorosi, A., Kowalewski, M., 2014. Quantitative bathymetric models for late Quaternary transgressive-regressive cycles of the Po Plain, Italy. The Journal of Geology 122, 649-670.
- Wright, V., 1992. A revised classification of limestones. Sediment. Geol. 76, 177–185. Yang, B., Steiner, M., Li, G., Keupp, H., 2014. Terreneuvian small shelly faunas of East Yunnan (South China) and their biostratigraphic implications. Palaeogeogr. Palaeoclimatol. Palaeoecol. 398, 28-58.
- Zang, W.L., Jago, J.B., Alexander, E.M., Paraschivoiu, E., 2004. A review of basin evolution, sequence analysis and petroleum potential of the frontier Arrowie Basin. In: Boult, P.J., Johns, D.R., Lang, S.C. (Eds.), Eastern Australian Basins Symposium II. Petroleum Exploration Society of Australia, Special Publication, South Australia, pp. 243-256.
- Zhou, B., Xiao, L., 1984. Early Cambrian monoplacophorans and gastropods from Huainan and Huoqiu counties, Anhui Province. Professional Papers of Stratigraphy and Palaeontology 13, 125-140.